UCLouvain

AGRO LOUVAIN

Faculté des bioingénieurs

Highly dispersed Keggin phosphomolybdates as deoxydehydration catalysts

Auteur : Sébastien Baffrey

Promoteurs : Eric M. Gaigneaux (UCLouvain) et Sophie Hermans (UCLouvain)

Encadrant : Alixandre Magerat

Lecteurs : Michel Devillers (UCLouvain) et Josefine Schnee (Sorbonne Université)

Année académique 2024-2025

Mémoire de fin d'études présenté en vue de l'obtention du diplôme de Bioingénieur : Chimie et bioindustries

Acknowledgements

Je tiens tout d'abord à exprimer ma profonde gratitude à mon encadrant, Alixandre Magerat, pour son rôle central dans la réalisation de ce mémoire. Sa guidance éclairée, ses conseils précieux, et son investissement, même dans des corrections de dernière minute, ont été déterminants. Ce travail n'aurait jamais pu voir le jour sans son soutien indéfectible. Je demeure admiratif de sa vaste connaissance des sources existantes sur la DODH (je défie quiconque de lui en présenter une qu'il ne connaîtrait pas !). Je lui adresse mes vœux de réussite pour l'achèvement de sa thèse et lui recommande avec insistance de rester éloigné des motos.

Je remercie également mes deux co-promoteurs pour leur accompagnement précieux tout au long de ce projet. Je suis particulièrement reconnaissant envers le Professeur Éric Gaigneaux pour le temps qu'il m'a accordé, répondant avec patience à mes nombreuses interrogations, parfois entre deux cours, et m'orientant avec des idées novatrices et des informations capitales. Mes remerciements s'adressent également au Professeur Sophie Hermans pour son expertise rigoureuse et ses interventions pertinentes, toujours constructives lors de nos réunions. Je leur suis profondément reconnaissant pour la liberté de rédaction qu'ils m'ont laissée et pour leur encadrement bienveillant.

Je souhaite aussi remercier François Devred pour son soutien technique infaillible et sa bonne humeur communicative. Je croise les doigts pour que Lille franchisse les 16e de finale de la Ligue des champions !

Mes remerciements vont également à Noé pour son expertise pointue sur le sujet et pour ses idées parfois véritablement « game changer », qui ont permis de débloquer des étapes clés de mon travail.

Je tiens à exprimer ma gratitude aux Professeurs Michel Devillers et Joséphine Schnee, qui ont accepté de juger la qualité de ce mémoire et de consacrer leur temps à la lecture et ma défense orale.

Enfin, je remercie chaleureusement mes proches ainsi que toutes les personnes qui ont contribué, de près ou de loin, à l'aboutissement de ce travail. Une mention toute particulière va à ma compagne, Calypso, pour sa patience et son soutien constant, allant jusqu'à feindre de comprendre mes explications pour m'encourager. Merci du fond du cœur, mon amour.

Table of contents

Abbreviations

ATR: Attenuated Total Reflectance

DODH: Deoxydehydration

FTIR: Fourier Transform Infrared Spectroscopy

H_3PMo: Phosphomolybdic acid ($H_3PMo_{12}O_{40}$)

ICP-AES: Inductively coupled plasma-atomic emission spectroscopy

ML (%ML): Monolayer percentage

NH_4PMo: Ammonium phosphomolybdate ($(NH_4)_3PMo_{12}O_{40}$)

PXRD: Powder X-ray Diffraction

TPD-NH_3: Temperature-Programmed Desorption of Ammonia

UV-Vis: Ultraviolet-Visible Spectroscopy

XPS: X-ray photoelectron spectroscopy

Introduction

Industrial chemicals remain predominantly derived from petroleum despite its finite nature. Petroleum resources have been increasingly depleting since the Industrial Revolution due to extensive fossil fuel usage [1]. On the contrary, biomass offers a promising alternative as it is a more abundant and renewable carbon source. Biomass regenerates 100,000 to 1,000,000 times faster than petroleum, which has taken millions of years to form [2]. However, biomass primarily consists of long and complex biopolymers (e.g. cellulose or lignin) characterized by a notably higher oxygen-to-carbon (O/C) ratio compared to fossil molecules [3]. For instance, while cellulose has an O/C ratio close to 1, this ratio approaches 0 in petroleum-derived hydrocarbons [4]. The high oxygen content of biomass represents a challenge for its integration into existing industrial processes, which traditionally consider the addition of functional groups to carbon chains rather than their removal [5]. For example, polyols (e.g. glucose, erythritol or sorbitol) are typical depolymerization products of biomass [6]. These molecules contain multiple hydroxyl groups which must be eliminated to produce functional intermediates better suited for chemical synthesis in processes optimized from olefins [7].

Indeed, olefins play a central role in chemical industry due to their high reactivity, which stems from the presence of a carbon-carbon double bond [7]. This feature gives them a chemical reactivity enabling a wide range of transformations such as addition, oxidation, polymerization, and hydrogenation reactions [8]. The double bond in olefins creates reactive sites that facilitate the introduction of various functional groups, a crucial aspect to produce specific chemicals and materials [5]. For example, olefins are particularly demanded in

the polymer industry for the production of polymers like polyethylene, polypropylene, and polyvinyl chloride (PVC) that are ubiquitous in plastics, textiles, and in the construction sector [7], [8]. Additionally, olefins are employed in the manufacture of fuel additives, lubricants, and surfactants, thereby enhancing the performance of finished products [7], [8]. In the pharmaceutical industry, they serve as precursors for the synthesis of drugs, where their ability to be functionalized allows for the creation of complex molecules necessary for biological activity [9]. All of this makes deoxygenation of biopolymers (or their depolymerization products) a crucial step for adapting biomass derivatives to current industrial applications.

Deoxydehydration (DODH) is a key reaction addressing this need. DODH (Figure 1) converts vicinal diols into olefins and a water molecule by using a sacrificial reductant and a catalyst [5]. DODH is particularly advantageous as it combines deoxygenation and dehydration in a single step, making it a highly efficient approach for producing olefins from polyols. This dual functionality makes DODH relevant for incorporating biomass-derived molecules into modern chemical manufacturing.

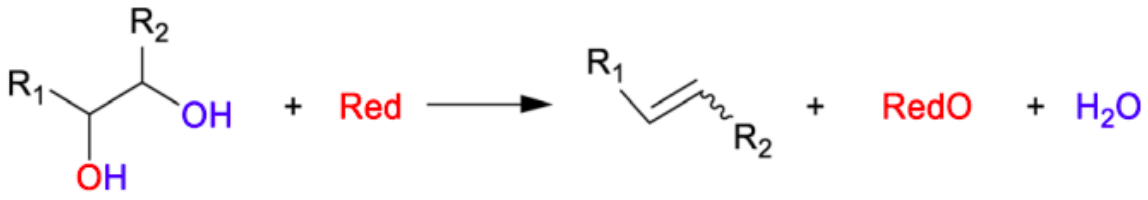

Figure 1: Deoxydehydration of a vicinal diol into an olefin. Red = Reductant. RedO = Oxidized reductant.

Catalysts capable of performing DODH typically employ intermediate transition metals such as Re, Mo, or V, due to their balanced oxophilicity [5]. Late transition metals exhibit insufficient oxophilicity to effectively extract oxygen from organic molecules, while early transition metals form overly strong bonds with oxygen. Re catalysts are the gold standard for catalyzing DODH as they have shown superior catalytic performances. These very good performances are attributed to the wide range of oxidation states that Re can adopt and to its strong ligand-binding capabilities [10]. However, its high price – which mirrors its extreme scarcity (about 10^{-3} ppm in Earth crust [6]) – has driven the development of catalysts based on more abundant metals, like V and Mo (100 and 1 ppm Earth crust abundance, respectively [6]). Mo-based catalysts perform better than V-based ones, as vanadium requires a specific environment to achieve high olefin yields [11].

State of the Art

Mechanism

The DODH mechanism is generally described as a series of three substeps [5] [12], regardless of the catalyst nature (Figure 2): (1) the initial formation of a diolate (or glycolate) complex via coordination of the vicinal diol to the catalyst (a redox-neutral condensation step), (2) reduction of the metal-oxo-diolate complex by a reducing agent, and (3) the extrusion of the alkene product alongside with the catalyst regeneration in a retrocyclization step. Importantly, steps (1) and (2) can occur in inverted order, giving rise to two potential pathways, with the sequence being catalyst- and reductant-dependent. The rate-determining step varies depending on both components.

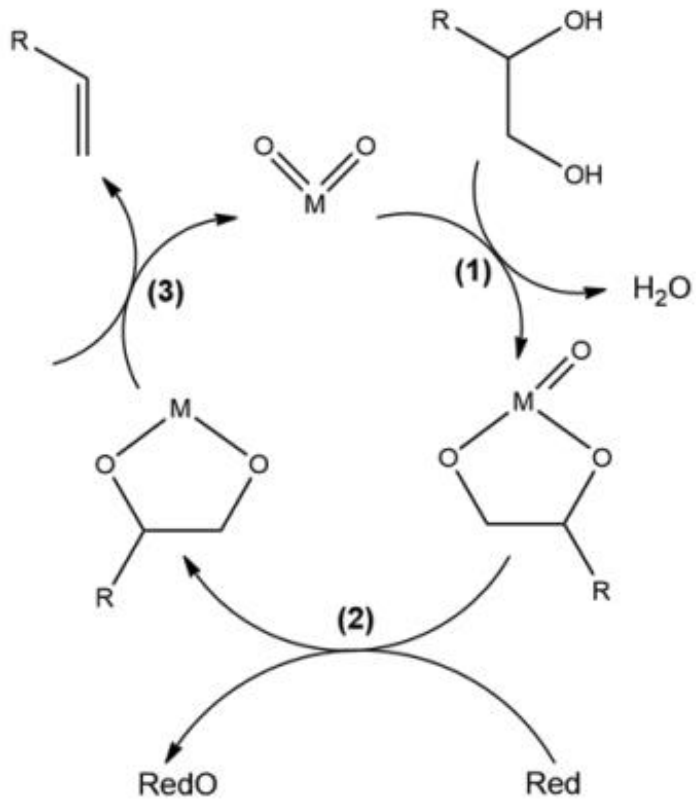

Figure 2: DODH generic mechanism. M = high-valent transition metal. Red = Reductant. RedO = Oxidized reductant.

Figure 2 actually simplifies the reduction process, as this specific step can differ based on the catalyst and reductant selected. Typically, three main types of reduction mechanisms are reported: (1) oxo-extraction, (2) transfer hydrogenation, and (3) oxidative cleavage of the substrate [13]. The oxo-abstraction mechanism depicted in Figure 2 illustrates reduction of the metal-diolate complex, which usually occurs with a reductant such as triphenylphosphine (PPh_3). Transfer hydrogenation often employs a secondary alcohol as the reductant such as 3-octanol. In this process, the alcohol is oxidized into the corresponding ketone or aldehyde, resulting in the release of a water molecule (Figure 3a).

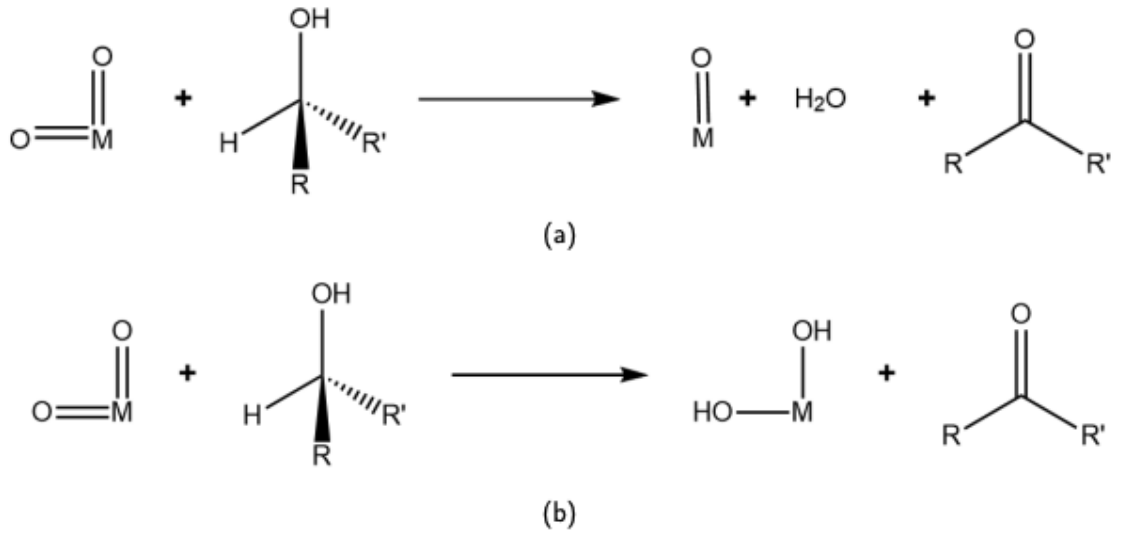

Figure 3: Transfer hydrogenation mechanisms in DODH. (a) Transfer hydrogenation yielding an oxo-metal center and (b) Transfer hydrogenation yielding a dihydroxy-metal center. M = high-valent transition metal.

Hydrogenation of two oxido ligands with the formation of OH ligands is also possible (Figure 3b) [14]. In some cases, the diol substrate itself can act as the reductant (Figure 4), wherein C-C bond cleavage in the diolate complex yields two carbonyl compounds (ketones or aldehydes). These products may further react with alcohols through acetalization. Since the latter is acid-catalyzed, oxidative cleavage of diols tends to be favored under acidic conditions (see appendices Figure A). Additionally, this oxidative cleavage pathway has an inherent 50% limit on alkene yield and can lead to complex reaction mixtures. This pathway is more prominent at high temperatures (200–250°C), particularly when molybdenum-based catalysts are used [15].

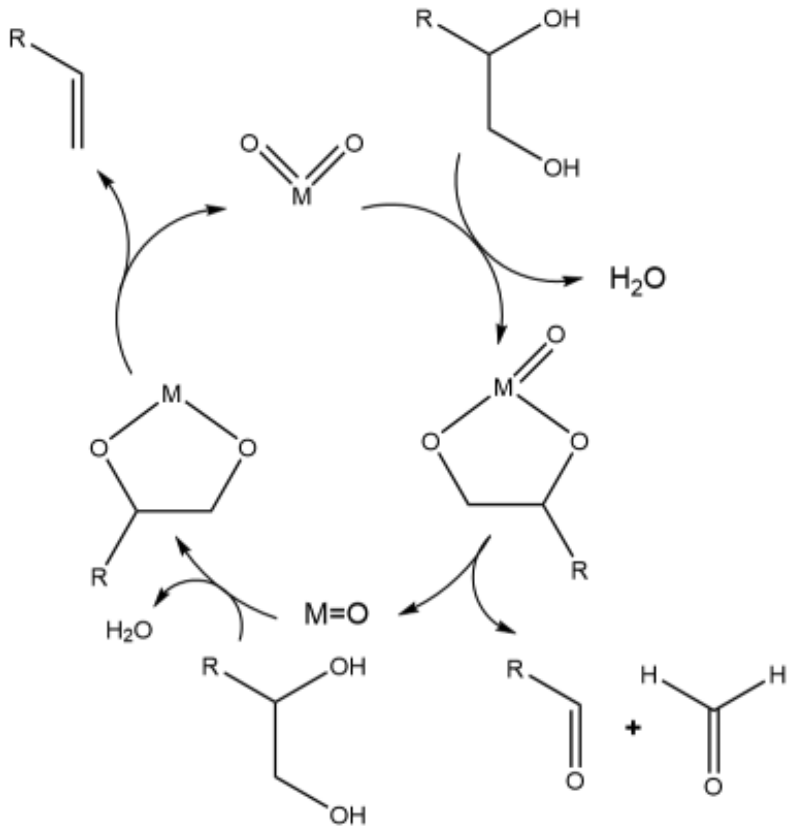

Figure 4: Reduction of the catalyst by oxidative cleavage of the diol. M = high-valent transition metal.

Reductants

With one single exception reported today [16], sacrificial reductants are always needed to perform DODH. The choice of reductant in DODH plays a critical role in determining the efficiency, selectivity, and feasibility of the process. Reductants can be broadly categorized into 3 types, based on how the reduction step is performed: oxygen-extracting agents, hydrogen-transfer agents and oxidative cleavage agents, in which latter case it is generally performed by the substrate itself. The first two types of reductants are named "external" reductants, whereas the third one is qualified as "internal". Table 1 summarizes some common reductants categorized into these 3 groups. While these illustrate the primary mechanisms, other less common pathways also exist [5].

Table 1: Several examples of some common reductants for DODH.

Category	Reductant	Oxidized Form	Ref.
Oxygen-Extraction Agents	PPh_3	$OPPh_3$	[17]
	CO	CO_2	[18]
	Na_2SO_3	Na_2SO_4	[19]
	H_2	H_2O	[17]
Hydrogen-Transfer Agents	1-Butanol	Butanal	[20]
	2-Nonanol	2-Nonanone	[21]
	Cyclooctanol	Cyclooctanone	[21]
Oxidative cleavage agents	1,2-hexanediol	Pentanal and methanal	[22]

In DODH, strong reductants typically ensure high olefin yields, though side reactions, such as over-reduction of the catalyst or product, and unintended reduction by the diol can lower the overall efficiency of the process. Reductant selection is based on substrate properties, economic factors, and sustainability. The reductant interaction with the catalyst is critical, but uncertainties remain about whether reduction targets the catalyst directly or an intermediate complex, complicating the choice [5].

Oxygen-Extracting Reductants

Oxygen-extracting reductants operate by removing oxygen from the diol substrate, typically forming a stable oxidized byproduct. For instance, triphenylphosphine (PPh_3), one of the earliest and most used reductants for DODH, reacts to form triphenylphosphine oxide (PPh_3O). Variants such as tri-n-butylphosphine and triethylphosphine offer similar reactivity. These reductants are particularly effective in liquid-phase reactions under laboratory conditions. Other examples of oxygen-extracting reductants include gaseous reductants like carbon monoxide (CO), which forms CO_2, and dihydrogen (H_2), which produces water as a byproduct. These reductants are attractive because of their industrial availability. However, elevated pressures and a secondary catalyst or both may sometimes be required. For example, CO has been utilized at 13.8 bar with rhenium-based catalysts [23] and at 20 bar with vanadium-based catalysts [24]. Similarly, H_2 has been employed successfully at pressures ranging from 1 to 14 bar with rhenium catalysts [25], [26]. The activation of H_2 can be enhanced by incorporating a metal catalyst which can also generate atomic hydrogen [27]. This atomic hydrogen may lead to hydrogenation of the olefin product forming

a saturated compound [27], which is not always desired. This issue can be partially solved by using mild hydrogenation catalysts, such as gold [28].

Solid reductants, including metallic zinc, manganese, and iron, also fall into this category [29]. These reductants provide sufficient thermodynamic driving force but may suffer from poor solubility in organic solvents making them less active. Sodium sulfite (Na_2SO_3) has been successfully applied in DODH, with crown ethers sometimes added to enhance its solubility [30].

Hydrogen-Transfer Reductants

Hydrogen-transfer agents contribute hydrogen to the reaction, leading to the formation of water as a small, thermodynamically favored byproduct. Alcohols, including primary and secondary types, are commonly used as hydrogen-transfer reductants. Primary alcohols are oxidized to aldehydes, whereas secondary alcohols yield ketones, with the latter being thermodynamically more favorable due to the stability of ketone products. Several alcohols, such as 1-butanol and 2-hexanol, are considered sustainable reductants because they can be derived from biomass [31]. Notably, alcohols can also serve as both reductants and solvents, simplifying reaction conditions.

Diols as Internal Reductants

Diol substrates themselves can act as internal reductants, circumventing the need for an external reducing agent [5]. To validate the use of external reductants in such cases, the yield of olefins must exceed 50%, or the oxidized diol products must be carefully quantified to distinguish contributions from self-

reduction. But this is complicated because these oxidation products quickly react to form other compounds that are themselves difficult to identify [12].

Deoxydehydration catalysts

A wide variety of catalysts have been investigated for DODH. While it might seem straightforward to classify them into homogeneous and heterogeneous categories, this distinction is often blurred due to the prevalent issue of leaching observed in most heterogeneous catalysts [5]. In this context, the classification will instead be organized as follows: catalysts composed of active phase[1] only (non-supported catalysts) and supported catalysts.

Non-supported catalysts

Among non-supported catalysts, several cyclopentadienyl MO_x (M = Re or Mo) organometallic complexes have been tested by various researchers, though with limited success. This is likely due to agglomeration or oligomerization of the catalyst during the reaction [13]. However, other catalysts in different forms have also been explored. Table 2 highlights several examples tested under various conditions. Most show relatively low yields, though some achieve high values, often associated with the use of potent but environmentally unsustainable reductants or solvents. Notably, the third entry in the table stands out for its high yield while employing sustainable solvent and reductant. However, it relies on rhenium, a costly and scarce metal.

[1] In the absence of a study on the nature of the active phase, it is here assumed that the active phase corresponds to the one initially brought into contact with the reactants.

Table 2: Non-supported catalysts for the DODH reaction. The conditions column report systematically the reductant, the solvent, the temperature and the reaction time used for catalytic testing. Sometimes, the solvent served also as reductant.

Substrate	**Catalyst**	**Conditions**	**Yield (%)**	**Ref**
1,2-hexanediol	$(NH_4)_6Mo_7O_{24}$	iPrOH, 250°C, 13h20	55	[32]
diethyl tartrate	$[Bu_4N](dipic)VO_2$[2]	PPh_3, benzene, 170°C, 96h	85	[17]
erythritol	L[4]$Re(CO)_3$[3]	3-Octanol, 180°C, 3h	78	[33]

Supported catalysts

Supported catalysts have been extensively studied due to their potential for high-throughput production, which is particularly desirable in DODH of organic derivatives given the abundance of biomass. An ideal catalyst would be inexpensive, recyclable, and maintain stable activity.

Since non-supported rhenium-based catalysts demonstrate the most promising results, numerous research efforts have focused on supporting Re, predominantly as rhenium oxide (ReO_x) [34]. The initial supported catalyst attempts included ReO_x/C, synthesized from ammonium perrhenate (NH_4ReO_4)

[2] Tetrabutylammonium dioxo(2,6-pyridinedicarboxylato)vanadate
[3] 2-(((2-(dimethylamino)ethyl)(methyl)amino)methyl)phenol) $Re(CO)_3$

precursor [26]. Subsequently, various supports were investigated, including TiO_2. The work by Sandbrink et al. [35] demonstrated that ReO_x/TiO_2 remains recyclable up to seven times without activity loss, unlike when other supports are used such as SiO_2, carbon, or ZrO_2. Catalyst activation using H_2 appears to reduce leaching risks [35], [36]. Rhenium is also coupled with other noble metals (e.g. Au, Ag) to try enhancing catalytic performance [37] [28]. Table 3 compiles various supported catalysts tested with the reaction conditions being specified as well as the obtained yields.

Regarding molybdenum, it is similarly mostly supported on same supports as ReO_X (TiO_2, SiO_2, C…), though generally exhibiting lower yields [23]. Vanadium-based catalysts consistently demonstrate even inferior performance for DODH applications [5], [38]. Tungsten (W) exhibits catalytic activity in DODH reactions, however, it generally demonstrates lower selectivity compared to both molybdenum and vanadium catalysts [12].

Table 3: Supported catalysts for the DODH reaction. The conditions column report systematically the reductant, the solvent, the temperature and the reaction time used for catalysts testing. Sometimes, the solvent served also as reductant.

SUBSTRATE	CATALYST	CONDITIONS	YIELD (%)	REF
Diethyl tartrate	ReO_x/C	1.4 MPa H_2, benzene, 150°C, 48h	95	[26]
1,2-hexanediol	ReO_x/TiO_2	3-octanol, 170°C, 1h	46	[35]
1,2-hexanediol	ReO_x/SiO_2	3-octanol, 170°C, 1h	49	[35]
Glycerol	ReO_x/CeO_2 + Au/CeO_2	8 MPa H_2, 140°C	67	[28]
1,4-AE[4]	$(NH_4)_6Mo_7O_{24}\cdot 4H_2O/TiO_2$	3-Octanol, 200°C	48	[36]
1,2-Decanediol	MoO_x/TiO_2	PPh_3	17	[23]
1,2-Decanediol	MoO_x/SiO_2	PPh_3	15	[23]
2,3-Butanediol	VO_x/SiO_2	2,3-Butanediol, 400°C, H_2	37	[38]

[4] 1,4-Anhydroerythritol

Objectives and strategy

The primary objective of this study is to develop a catalyst that can effectively replace rhenium-based systems, addressing key industrial requirements: low cost, great abundance, minimal leaching, and stable catalytic activity over multiple recycling cycles. Keggin-type polyoxometalates (POMs) (Figure 5) are potential promising candidates to catalyze DODH as they present common characteristics to already-known DODH catalysts, such as a potential multiplicity of oxidized metal active sites.

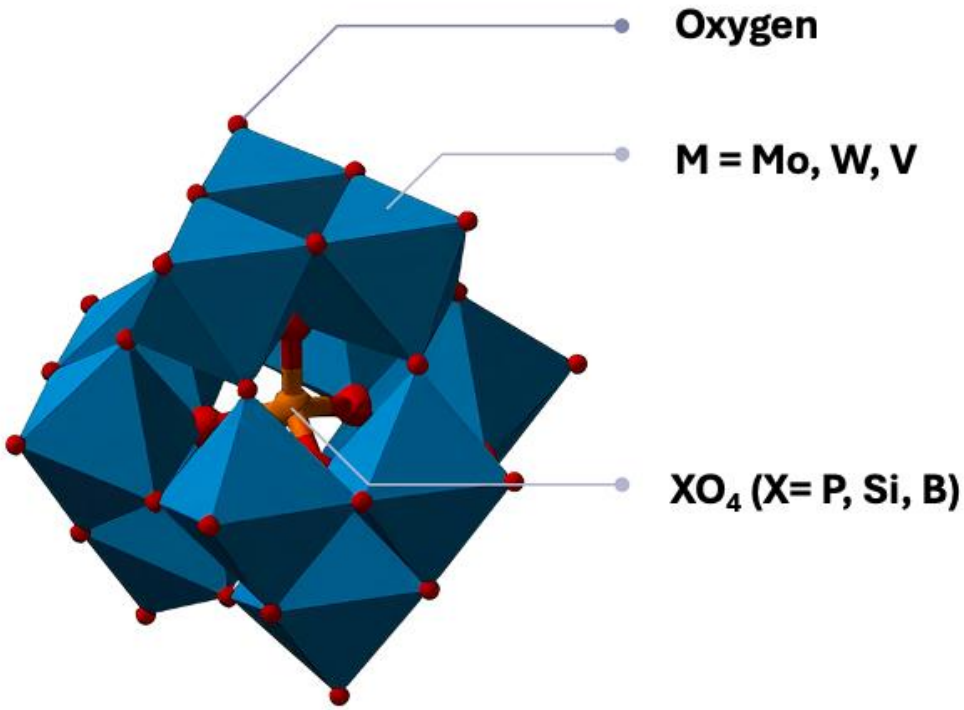

Figure 5: Structure of Keggin-type polyoxometalates (POMs).

Keggin POMs are well-defined molecular metal-oxide anions ($[XM_{12}O_{40}]^{n-}$) exhibiting a characteristic structural arrangement consisting of a central

tetrahedral XO_4 unit (where X can be ., Si, or other heteroatoms) surrounded by twelve MO_6 octahedra (where M typically is Mo, W, or V[5]) [39].

The robust framework of Keggin POMs offers several advantages [40], including:

- Relatively high thermal stability (most decompose between 350°C and 500°C) [40].
- Tunable redox properties by changing or substituting the metal M (e.g. $[PMo_6V_6O_{40}]^{9-}$) [40].
- Potential for changing cations to modify material properties, such as acidity, hydrophobicity, solubility, *etc*. [41].

Magerat et al. [42] compared the performance of 2 types of Keggin POMs, namely $PW_{12}O_{40}^{3-}$ and $PMo_{12}O_{40}^{3-}$ associated with different counter-cations: H^+, NH_4^+ and tetrabutylammonium (TBA^+) (Figure 6). Molybdenum-based Keggin polyoxometalates demonstrated superior catalytic activity compared to their tungsten counterparts in DODH. This enhanced performance might be attributed to the more favorable redox properties of molybdenum, namely its higher reducibility, as compared to tungsten [40], [43]. Among the cations, TBA brought the best performance for this reaction, but this will not be the subject of this work as already being studied by Alixandre Magerat. However, $(NH_4)_3PMo_{12}O_{40}$ (abbreviated as NH_4PMo) seems to have a higher selectivity than the acidic version H_3PMo ($H_3PMo_{12}O_{40}$) which makes it a candidate for further research, especially as it has interesting properties. The one that stands out is the fact that NH_4PMo is insoluble in many solvents (Ethanol, H_2O, dodecane, …) [44]. This property is interesting because it could potentially reduce leaching and allow the

[5] The mentioned metals are those capable of catalyzing DODH.

catalyst to be reused easily. Hence, NH_4PMo represents a novel candidate for DODH reactions, particularly noteworthy due to its potential recyclability.

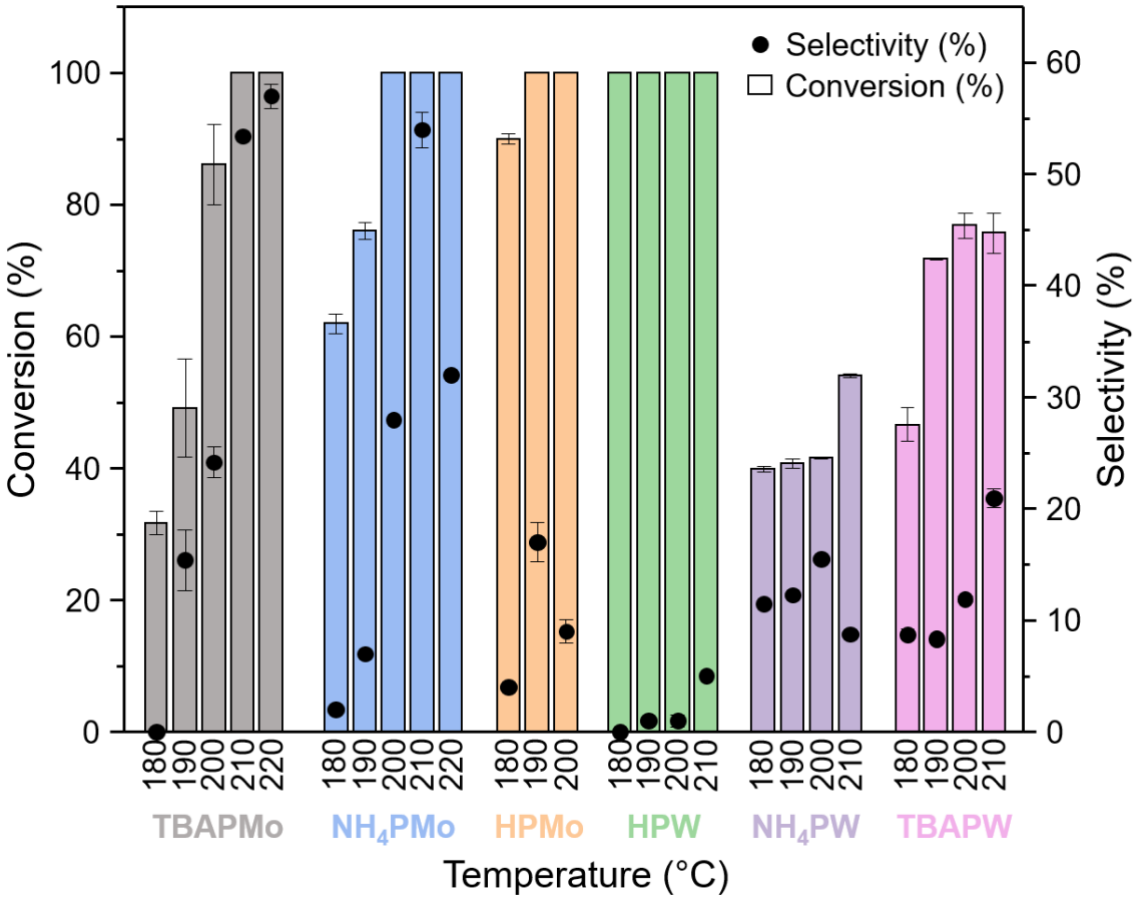

Figure 6: Catalytic results (conversion of 1,2-hexanediol, selectivity for 1-hexene) with different phosphododecamolybdates and phosphododecatungstates at different reaction temperatures and with different countercations (H^+, NH_4^+ and TBA^+). Reaction conditions: 5 mL of a solution containing 0.1 mol/L 1,2-hexanediol and 0.1 mol/L n-dodecane (internal standard), 15 mg of each powder, 18h at a given temperature [42].

Supporting this catalyst could potentially increase its dispersion and further facilitate catalyst recyclability. However, the direct wet impregnation of NH_4PMo is difficult due to its very low solubility (< 0.02g/100mL of water according to the supplier) in common solvents [45]. In addition, a deposition-precipitation synthesis would not be advantageous, as it would form NH_4PMo clusters with poor dispersion. On the opposite, Keggin heteropolyacids (HPAs) appear to disperse well on common supports. Schnee et al. demonstrated that the acid-base interaction of HPW ($H_3PW_{12}O_{40}$) on TiO_2 favored good dispersion [46]. Moreover, Keggin HPAs exhibit good dispersion on SiO_2 with reduced distortion despite the weaker interaction [47] [43], [48]. This behavior is attributed to the lower basicity of SiO_2 compared to TiO_2, resulting in a weaker interaction that minimizes structural deformation [49].

In summary, among Keggin-based catalysts, NH_4PMo offers the best performance for DODH (top-performing TBAPMo excluded). Furthermore, it is insoluble in most organic solvents encouraging more efficient recycling. Hence, a novel synthetic strategy considering the difficulty in supporting it by wet impregnation has been proposed utilizing the following approach:

1. Wet impregnation with the highly soluble phosphomolybdic acid (H_3PMo) on a support that allows easy dispersion without over-neutralizing the H_3PMo acidity making neutralization by NH_3 less favorable.

2. Subsequent neutralization via a gaseous ammonia (NH_3) flow treatment to form a well-dispersed and much less soluble NH_4PMo phase.

This methodology appears particularly promising given that H_3PMo is classified as a strong Brønsted acid, suggesting efficient neutralization kinetics [40]. But the choice of support is crucial, as it will bring advantages (strong adsorption may potentially prevent leaching) or disadvantages (neutralization of H_3PMo by the support, hence preventing NH_3 from reacting with the acid) by interacting with H_3PMo.

Objectives

Ultimately, the primary objective can be refined into two secondary objectives:

1. Validating the synthesis of a highly dispersed NH_4PMo catalyst on a solid support.
2. Demonstrating that this catalyst is both efficient and capable of maintaining stable activity over multiple recycling cycles for DODH reaction.

Strategy

The strategy to achieve these objectives will be divided into three phases.

Phase 1: Bulk NH_4PMo Catalyst Synthesis Optimization

The aim of this part of the work is to optimize NH_4PMo synthesis by NH_3 flushing on the bulk H_3PMo (not on supported H_3PMo), to facilitate characterizations and understanding. By comparison with NH_4PMo obtained commercially, two synthesis parameters will be varied: the temperature before (pretreatment) and after neutralization with NH_3 (post-treatment). The pretreatment was initially performed to maximize the drying of the sample, based on the assumption that water hinders the NH_3 from accessing the acidic sites. Variations of the pretreatment temperature were also made for comparison. The post-treatment is conducted to, (1) by analogy to what has been done with $H_3PW_{12}O_{40}$, [41] homogenize the sample by distributing NH_3 molecules over each available H^+, ensuring the formation of $(NH_4)_3PMo_{12}O_{40}$ for each molecule and to (2) desorb any excess NH_3 potentially adsorbed on the NH_4^+ sites of the newly formed NH_4PMo. The neutralization (carried out by flushing NH_3 through the powder) will always take place at room temperature, as adsorption is always exothermic. Next, each synthesis product obtained with these different conditions will be characterized – and compared with the commercial version – by PXRD (powder X-ray diffraction), infrared spectroscopy and UV-Vis spectroscopy.

Phase 2: Supported Catalyst Development

In this second part, H_3PMo will be impregnated on 2 different supports and subsequently neutralized with NH_3 following the protocol developed in stage 1. SiO_2 and TiO_2 will be used as support, as H_3PMo disperses well on them [46] [47] [43], [48]. Different loadings will be tested: 10% ML and 70% ML (%ML =

percentage of the theoretical surface area fraction covered by a monolayer (=ML) of H_3PMo). The support-H_3PMo interactions will be analyzed via TPD-NH_3 and cross-referenced with the literature. PXRD will be used to characterize (1) the dispersion and (2) the secondary structure of the supported phase whereas IR will be used to check the preservation of the Keggin structure. Finally, the solubility of all samples will be evaluated by UV-Vis spectroscopy.

Phase 3: Catalytic Performance Evaluation and Leaching Study

The aim of this third part of the experimental work will be to study the catalytic activity of the selected catalysts and the commercial bulk H_3PMo and NH_4PMo versions, checking whether there is any leaching and whether any activity is retained after repeated recycling. It will consist of 3 stages:

1. Catalytic tests

Catalytic tests will be carried out for the bulk (commercial H_3PMo and NH_4PMo) and supported versions (H_3PMo /support and NH_4PMo/support, support = TiO_2 or SiO_2 at different loadings (10 or 70% ML)).

2. Recycling

The H_3PMo and NH_4PMo bulk versions will first be recycled to see if recycling is possible for each sample. Then all supported catalysts will be recycled too, to see whether there is any loss of activity along the recycling. Acidic (H_3PMo /support) and neutralized (NH_4PMo/support) versions will be compared. These recycled catalysts will be analyzed by IR spectroscopy to observe any changes in the active phase.

3. Leaching study

The occurrence of leaching will be scrutinized using cold filtration tests. All catalysts tested in 1 will be addressed for this purpose.

Materials and methods

Materials

1,2-hexanediol (98%), phosphomolybdic acid hydrate ($H_3PMo_{12}O_{40}\cdot nH_2O$, >99%), ammonium phosphomolybdate hydrate ($(NH_4)_3PMo_{12}O_{40}\cdot nH_2O$, >99%) were purchased from Sigma-Aldrich. TiO_2 (P25, 50 m^2/g) and SiO_2 F320 (150 m^2/g,) was purchased from Degussa. 3-octanol (>98%) was purchased from Tokyo Chemical Industry (TCI). Absolute ethanol (>99%), n-hexane (>97%) and n-dodecane (100%) were purchased from VWR CHEMICALS. Nitrogen and oxygen are alpha 1 purity and ammonia 5% by volume (v/v) in Argon or Helium alpha 1 as well. All gases were purchased from Air Liquide. Potassium bromide for IR spectroscopy (≥99%) was obtained from Acros Organics.

Methods

Wet impregnation of $H_3PMo_{12}O_{40}$ into solid supports

To a 250 mL round-bottom flask containing 100 mL of ethanol, 1 g of support was suspended. The suspension was sonicated for 15 minutes. Then, a 20 mL solution containing a certain quantity (depending on the aimed loading) of dissolved $H_3PMo_{12}O_{40}\cdot 6H_2O$ (i.e. dried under vacuum <30 mbar at 25°C to remove physisorbed water) was added dropwise to the suspension. The mixture was then stirred for 2h before removing the solvent with a rotary evaporator (40°C, 280 rpm). The amount of H_3PMo added is calculated as a function of loading, and assuming a Keggin anion as a sphere of 1 nm in diameter. Hence, the surface occupied by 1 Keggin unit is a disk of 1 nm in diameter, i.e. 0.7854 nm^2. Thus, depending on the specific surface area of the support and on the aimed theoretical surface coverage (= % ML, the theoretical surface area fraction covered by a monolayer of H_3PMo) the corresponding calculated mass of H_3PMo

was added. For example, in the case of SiO_2, which has a specific surface area of 160 m^2/g, here is the calculation of the mass of H_3PMo to work with to reach 10% ML:

$$anion\ disk\ surface\ (ads) = \left(\pi \times \frac{D}{2}\right)^2$$
$$= (\pi \times 0.5\ nm)^2$$
$$= 7.85 \times 10^{-19}\ m^2$$

$$Nb = 0.1 \times \frac{160\ m^2}{ads} = 2.04 \times 10^{19}\ anions$$

$$W_{HPMo} = \frac{Nb}{N_A} \times MM_{HPMo} = 0.0654\ g$$

Where:

Nb = number of anions to cover 10% of the surface of SiO_2

W_{HPMo} = mass of active phase required to cover 10% of the surface of SiO_2 with a monolayer [g]

MM_{HPMo} = molar mass of H_3PMo hexa-hydrated = 1933.5 [g/ mol_{HPMo}]

N_A = Avogadro number = 6.022 x 10^{23} [anions/mol_{HPMo}]

Neutralization of H_3PMo -supported powders

H_3PMo (bulk or supported, 250 mg of bulk H_3PMo, 440 mg of supported H_3PMo) pre-dried under vacuum (<30 mbar) overnight at 25°C was inserted in a U-shaped chemisorption glass tube equipped with a frit glass and placed in a muffle furnace. Several conditions were tested. In the case a pre-treatment was carried out, a N_2 stream (40 mL/min) was flowed through the powder at 100°C or 300°C for the time required to reach the desired temperature at a rate of 5°C/min plus 1h. Then, the reactor was allowed to cool down to room temperature. The powder was then submitted to a NH_3 (5% vol. in He or Ar, 40 mL/min) stream

during 1 hour at room temperature (25°C). In the case of homogenization through post-treatment, the reactor is put into bypass mode and heated to 50/150/300°C for the time required to reach the desired temperature at a rate of 5°C/min plus 2h. The number of moles of NH_3 flowing through the powder during the neutralization was calculated using the ideal gas law and compared with the maximum number of moles of H_3PMo (calculated based on the maximum weight of H_3PMo in the reactor = 250 mg). The ratio $mole_{NH3}$/**3** x $mole_{HPMo}$ = 65.8 (**3** in the denominator is added because 3 molecules of NH_3 are required to neutralize the 3 protons in the H_3PMo molecule). Ammonia is therefore in very large excess to neutralize all the protons in the reactor.

Catalytic tests

In a closed pressure tube (LaborXing) equipped with a PTFE stir bar, a 3-octanol solution containing 0.1 mol/L of 1,2-hexanediol and 0.1 mol/L dodecane (internal standard) was added together with the solid catalyst respecting a ratio Mo/Diol of 5% mol. at 210°C. The model reaction is illustrated in Figure 7. After 18h of catalytic test, the tube was cooled down in an ice-water bath. The solution was then collected using a 1 mL syringe and the catalyst was separated using a filter (0.2 µm pore size syringe filter). The filtered solution was collected in a single 2 mL vial. Consequently, only one measurement is performed at the end of the catalytic test. Reactants and products were quantified using a GC-2010 Plus equipped with FID-2010 Plus detector, an SH-RTX-5 (30 m length, 0.25 mm inner diameter, 0.1 µm film thickness) column, an AOC-20s auto-sampler and an AOC-20i auto-injector from Shimadzu. A 1 µL aliquot of the prepared vial was injected (injector temperature: 275°C, 70°C for 6 min and then 20°C/min until 100°C, gas flow: 30 mL/min He, 40 mL/min H_2 and 400 mL/min dry air) and the analysis was performed in split mode (split = 15, inlet pressure = 25 psi). The

conversion and selectivity were calculated as described in equations 1 and 2, respectively. Concentrations were obtained using calibration curves established with pure commercial standards.

$$Conversion = \frac{(C_{diol})_{t=0} - (C_{diol})_{t=t*}}{(C_{diol})_{t=0}} \quad (1)$$

$$Selectivity = \frac{(C_{olefin})_{t=t*}}{(C_{diol})_{t=0} - (C_{diol})_{t=t*}} \quad (2)$$

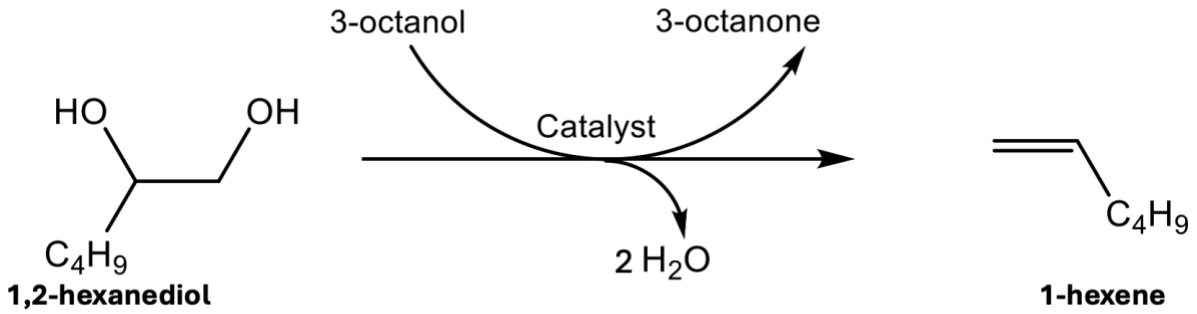

Figure 7: DODH model reaction used in this work for catalytic testing.

Cold filtration tests

To investigate the potential leaching of DODH active species, a catalytic test was initiated as described previously, with the exception that the reactor was cooled down during the "kinetic regime" (*viz.* before reaching a constant conversion over time). The solid catalyst was then removed from the reaction medium by filtration (0.2 µm pore size syringe filter) and the liquid fraction was placed again

under the same conditions as before cooling. The conversion and selectivity were monitored by GC to determine whether they continued to increase or remained constant after removal of the solid catalyst.

Recycling test

A catalytic test was performed during 5h as described above, except that at the end of the test, the catalyst was recovered by centrifugation (1 h, 14,000 rpm), washed 3 times with approximately 20 mL of n-hexane distributed across the 3 washings, and then dried overnight under vacuum (<20 mbar) at room temperature. The recovered and dried catalyst was then reused for another catalytic test in the same conditions. As mechanical losses are unavoidable, the volume of the reaction medium was reduced proportionally to the remaining mass of catalyst, assuming that these losses are homogeneous.

1. Instrumental

1.1 Infrared spectroscopy (IR)

All spectra were recorded on a Bruker INVENIO S equipped with a dielectric DTGS detector with an iris aperture of 5000 µm. 32 scans were recorded within approximately 10 seconds in the range 400–4000 cm^{-1} with a spectral resolution of 4 cm^{-1}.

1.1.1 Fourier transform infrared spectroscopy (FTIR, in the transmittance mode)

A spatula tip of powder was diluted in 150 mg of dry KBr and pressed into self-supporting wafers. A pure 150 mg KBr wafer was also analyzed and used as background.

1.1.2 Attenuated total reflectance (ATR) infrared spectroscopy

The ATR module housed by the IR spectrometer was used. Air was used as background in this case. A small amount of powder was placed on a very refractive diamond crystal and then slightly pressed against it before recording the spectra under the same conditions.

1.2 Ultraviolet-visible spectroscopy (UV-vis)

20 mg of each powder is mixed in 20 mL of ethanol, then each solution is filtered (0.2 µm pore size syringe filter) and analyzed using a Shimadzu UV-3600 Plus Series spectrometer with quartz High Precision Cells from Hellma Analytics. The spectra were recorded from 200 nm to 800 nm, with a 0.5 nm sampling interval and a slit width of 2 nm. For the 200-380 nm range, a deuterium lamp from Shimadzu was used as the light source, while a tungsten halogen lamp was used for the remainder of the spectrum.

1.3 Powder X-ray Diffraction (PXRD)

Powder X-ray diffraction patterns were recorded using a Bruker-D8 Advance diffractometer in Bragg-Brentano geometry. The X-ray source was a copper anode operated at 40 kV (Mean of $K\alpha_1$ and $K\alpha_2$ = 0.15418 nm) and 30 mA. The detector was a LynxEye XE-T. The 2θ angle was scanned from 5° to 80° at a speed of 5.93°/min (5051 steps of 0.015°). Well-ground powder samples were dispersed on a "zero noise" sample holder coated with Vaseline prior to insertion into the apparatus.

1.4 NH_3-TPD analysis

The NH_3 temperature-programmed desorption (TPD) experiments were performed using the CATLAB-PCS (Hiden Analytical) instrument equipped with a

QGA mass spectrometer (Hiden Analytical). The samples were initially heated at 300°C at a rate of 10°C/min for 1.5 h + the time to reach 300°C = 27.5 min (under an argon flow of 30 mL/min). Subsequently, adsorption was performed at 60°C for 1.5 h using a 5% v/v NH_3 in helium mixture (15 mL/min) supplemented with 15 mL/min of argon. Desorption was then carried out by heating the samples from 60°C to 700°C at a rate of 10°C/min under an argon flow of 30 mL/min.

Phase 1: Bulk NH_4PMo Catalyst Synthesis Optimization

In this phase, various synthesis conditions were tested to synthesized bulk NH_4PMo by NH_3 flushing starting from bulk H_3PMo. Table 4 lists the sample codes/names for each synthesis. The samples are denoted as X-NH_3-Y, where X indicates the pre-treatment condition/temperature, and Y represents the post-treatment temperature. The central NH_3 indicates the NH_3 neutralization during 1h that was consistently performed at 25°C. All powders were vacuum-dried (<30 mbar) at 25°C overnight before synthesis. If Y equals 25°C, the powder was simply recovered at room temperature after neutralization.

Table 4: Representation of the different NH_4PMo synthesis conditions.

Pretreatment is varied	Post-treatment is varied
100°C-NH_3-25°C	Vacuum 25°C-NH_3-50°C
300°C-NH_3-25°C	Vacuum 25°C-NH_3-150°C
Vacuum 25°C-NH_3-25°C	Vacuum 25°C-NH_3-300°C

Results

PXRD

Pretreated samples were analyzed by PXRD and their diffractogram were compared with the commercial NH_4PMo (reference) and commercial H_3PMo (Figure 8). Samples pretreated at 100°C and 300°C were amorphous, while the vacuum-dried sample exhibited a diffractogram similar to the one of the NH_4PMo reference.

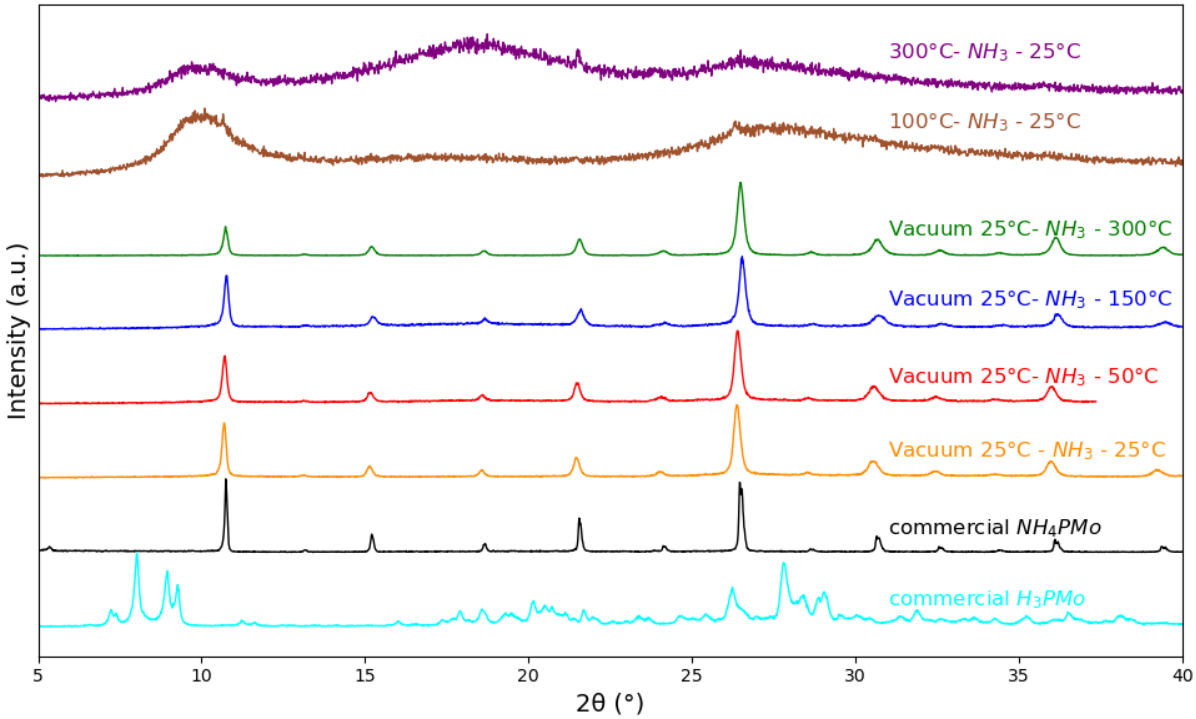

Figure 8: PXRD diffractograms of pretreated and posttreated samples compared with the commercial NH_4PMo and H_3PMo.

Posttreated samples were also analyzed. Their diffractograms were similar to the one of the commercial NH_4PMo (Figure 8). A slight shift ($\Delta 2\theta = 0.15$) compared to the reference can be observed (Figure 9), with the best alignment identified for the sample post-treated at 300°C.

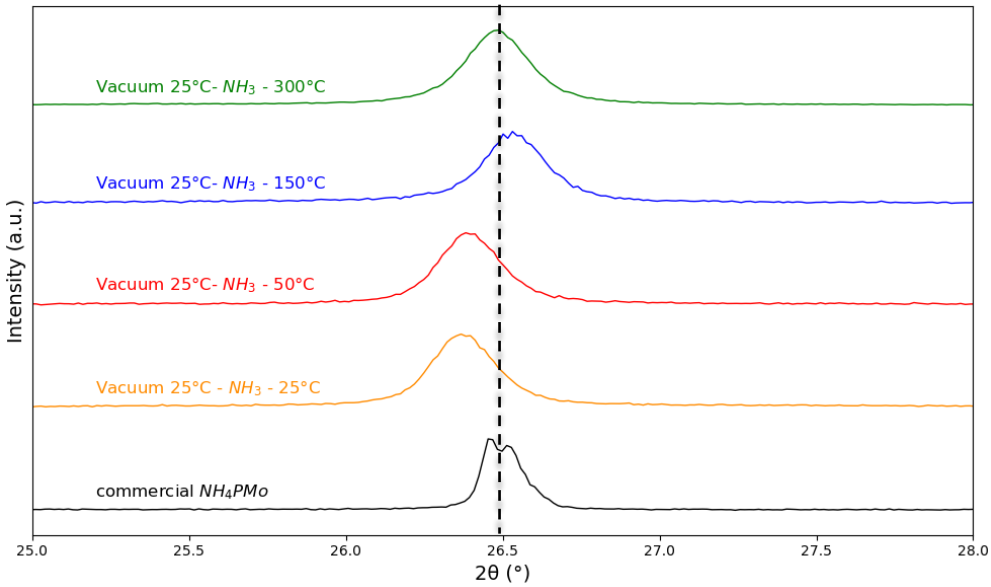

Figure 9: PXRD diffractograms (zoom on the peak at 26.5°) of posttreated samples compared with NH_4PMo.

UV spectroscopy

Each sample (20 mg) was mixed together with 20 mL of ethanol. The obtained suspension was then filtered out and the UV spectrum of the liquid fraction was recorded.

Pretreated powders (purple and cyan) showed very high absorbance as compared to the reference (black) (Figure 10). Conversely, spectra of posttreated powders exhibited absorbance closer to the reference' UV spectrum (Figure 11). The sample posttreated at 300°C (green) exhibits the lowest absorbance among all the samples.

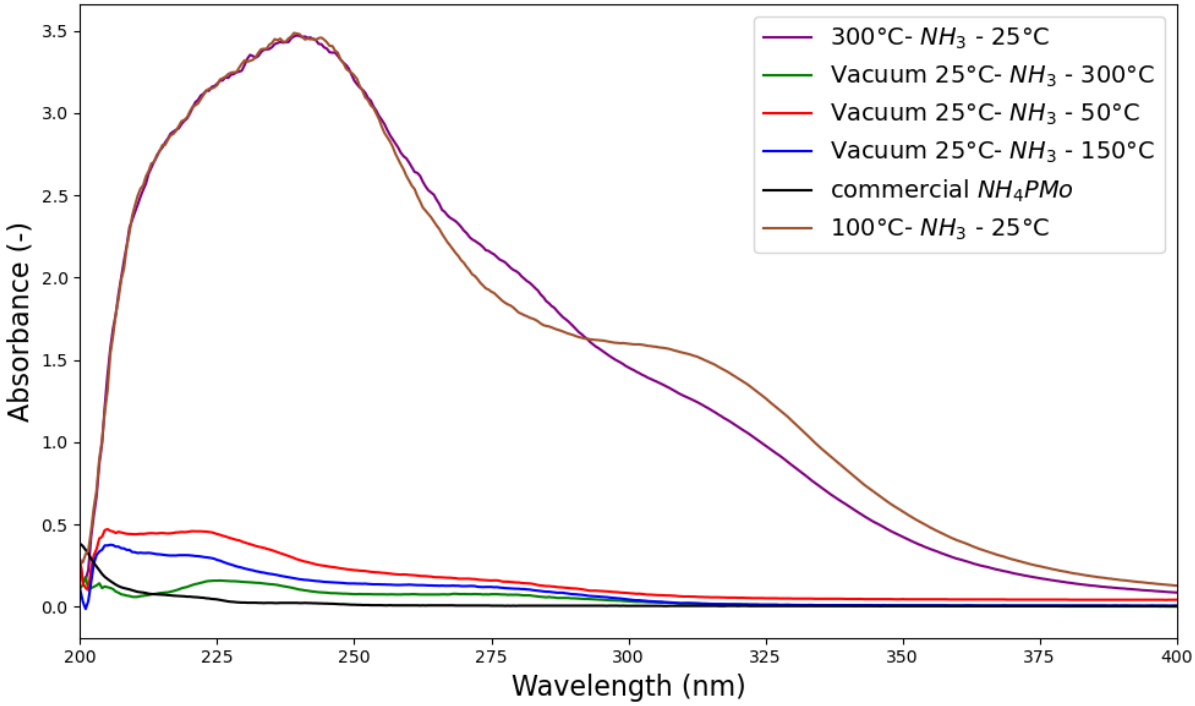

Figure 10: UV spectra of synthesized samples after filtration compared to the NH_4PMo reference (black).

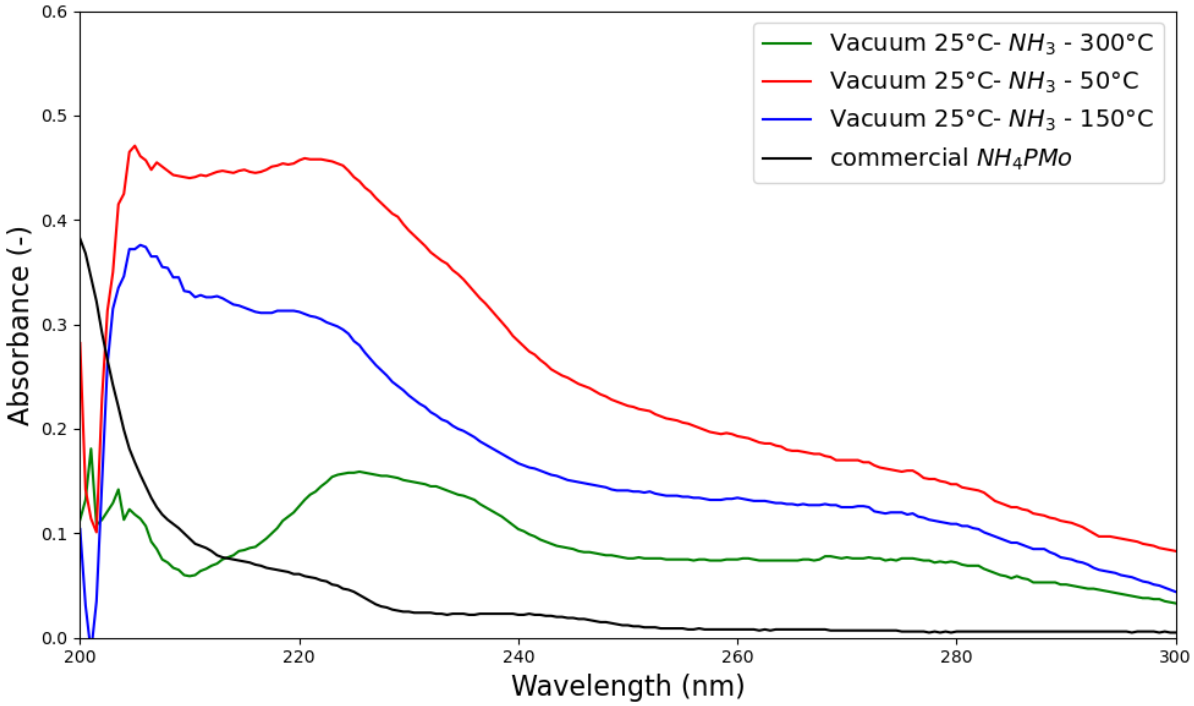

Figure 11: UV spectra comparing post-treated samples after filtration.

Infrared spectroscopy

ATR-IR spectroscopy was performed to check whether the Keggin structure was preserved. Only posttreated samples were analyzed and compared to the NH_4PMo reference because its UV results indicate a decreased solubility compared to the pretreated sample. The infrared spectra reveal four peaks, varying in intensity depending on the sample (Figure 12). Peaks at 1061 cm^{-1}, 960 cm^{-1}, 862 cm^{-1}, and 786 cm^{-1} are attributed to the asymmetric stretching vibrations of P–O, Mo=O, inter-octahedral Mo–O–Mo , and intra-octahedral Mo–O–Mo bonds, respectively [50]. The peak at 1406 cm^{-1} corresponds to the symmetric stretching vibration of the N–H bond [50]. The P–O peak at 1061 cm^{-1} shows a peak broadening decreasing with the increase of the posttreatment

temperature (Figure 13). Consequently, the sample posttreated at 300°C (green) closely resembles to the reference.

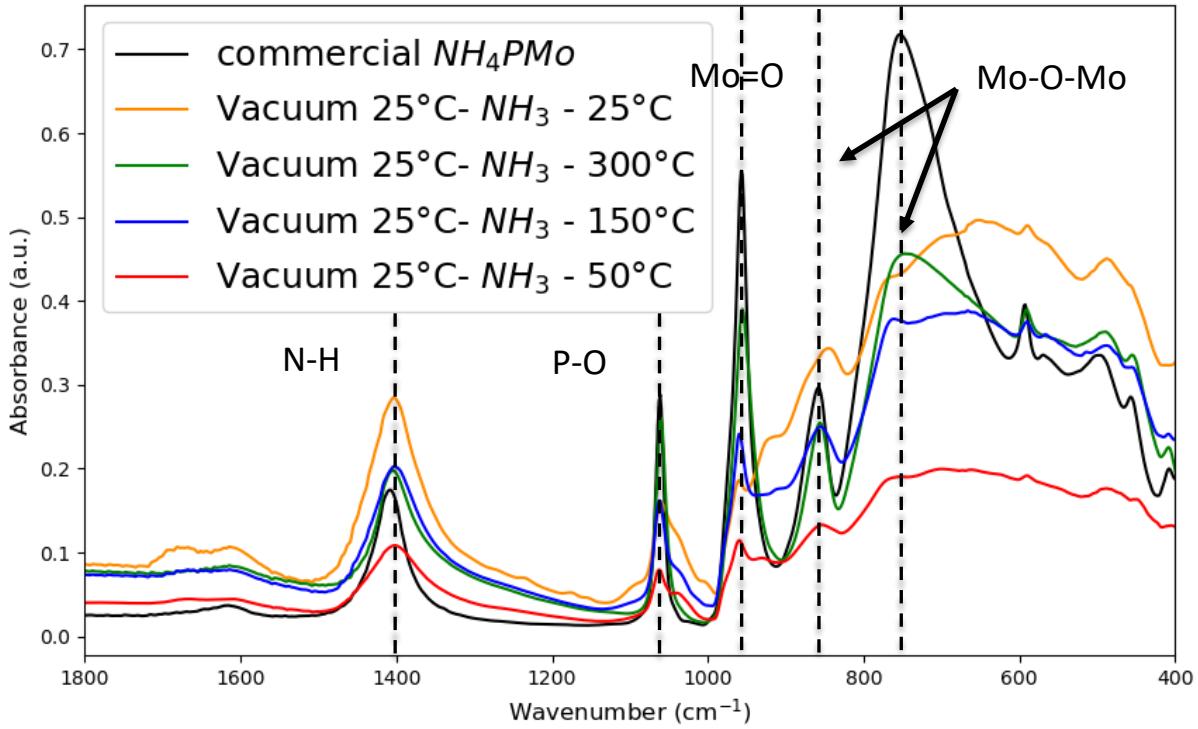

Figure 12: ATR-IR spectra of posttreated samples compared to NH_4PMo reference.

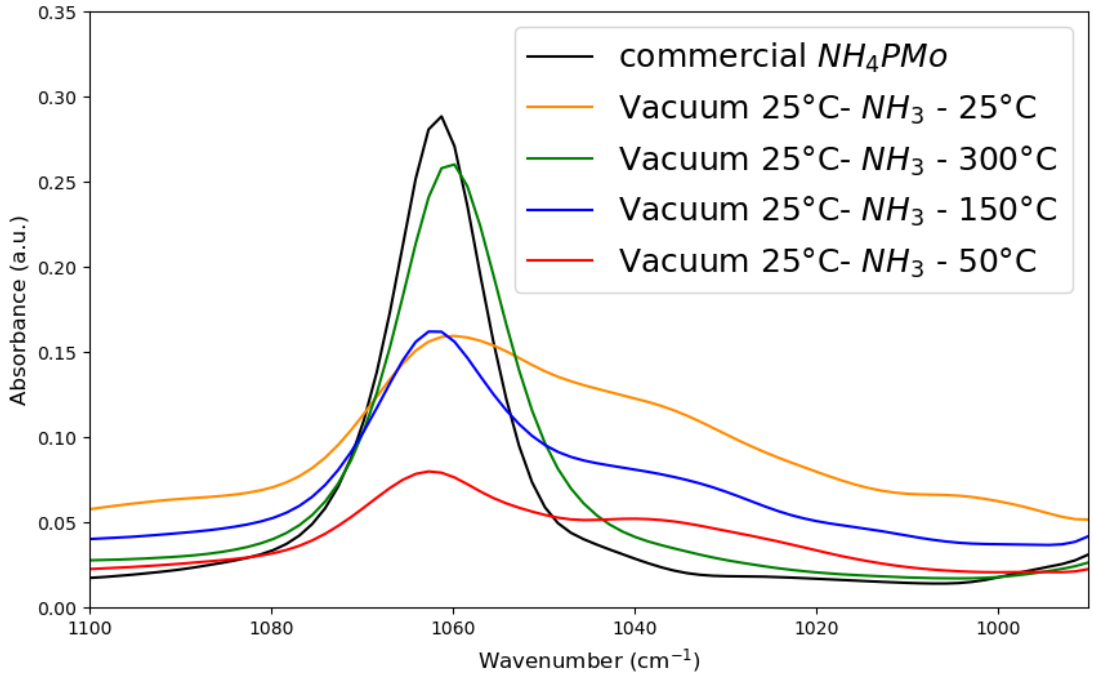

Figure 13: ATR-IR spectra of post-treated samples focusing on the P-O bond peak at 1061 cm^{-1} compared to NH_4PMo reference.

The areas under the peaks of the N–H and P–O vibrations at 1405 cm^{-1} and 1061 cm^{-1}, respectively, were quantified to obtain an N–H/P–O ratio. This ratio decreases as the posttreatment temperature increases (Figure 14). The ratio for the commercial NH_4PMo (= 2) and the sample posttreated at 300°C (=1.96) are almost the same, indicating a relatively similar number of N-H vibrations between the two.

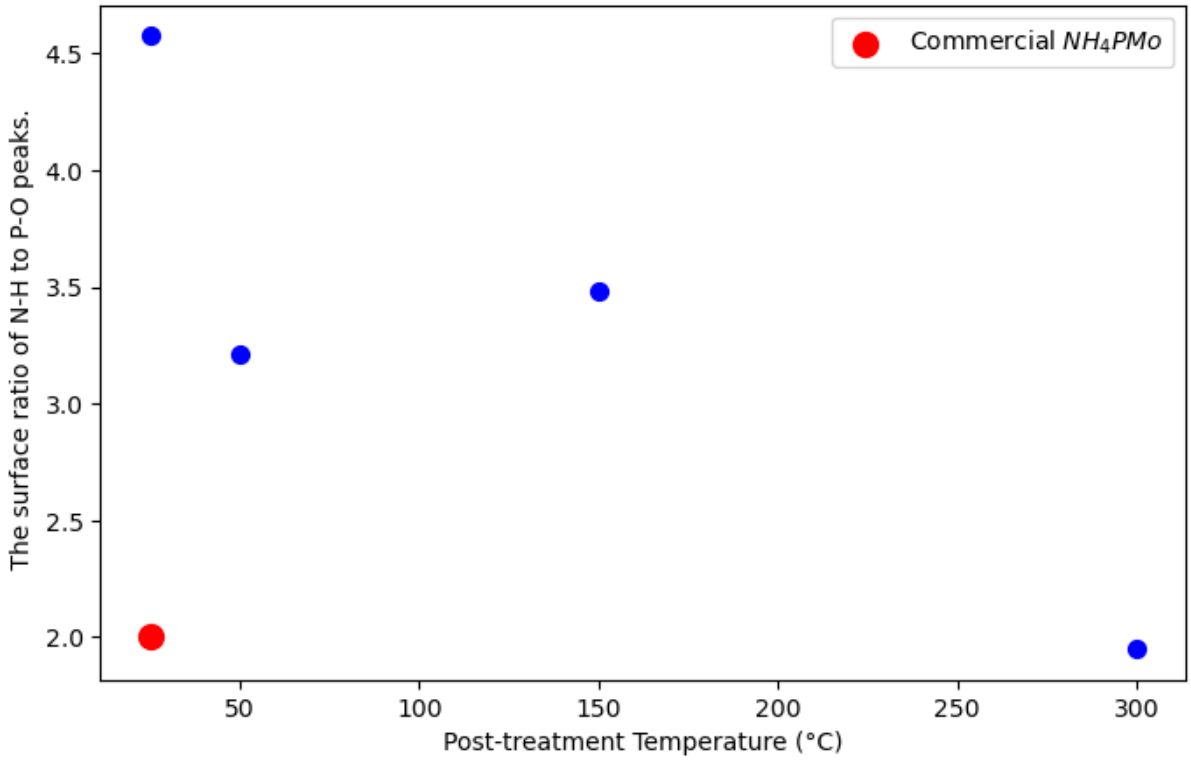

Figure 14: N–H/P–O ratio based on peak areas of pos-treated samples as a function of temperature.

Discussion

The PXRD patterns of pretreated samples showed no crystallinity. In contrast, the sample subjected only to vacuum drying at 25°C exhibits a diffractogram nearly identical to the desired commercial NH_4PMo reference. This indicates that pretreatment makes the samples amorphous. Posttreated samples show diffractograms comparable to the reference. The shifts observed in samples post-treated at 50°C and 150°C may result from the presence of residual water or NH_3, causing distortions linked to atomic displacement variations [51].

The UV analyses presented above confirm that posttreatment is more effective in producing samples with solubility properties close to the reference. However, one could observe that the peaks positions of the posttreated samples are not matching with the commercial NH_4PMo. This could be attributed to potential non-neutralized acidic sites or intermediate species/pollutants that might become soluble. Still, increasing the posttreatment temperature appears to reduce solubility.

ATR-IR results confirm the preservation of the Keggin structure in all posttreated samples. They also highlight a peak broadening in the P–O region. A suggested hypothesis could be that NH_3 molecules initially neutralize H_3PMo's protons to form NH_4^+ species, which subsequently adsorb additional NH_3 molecules. Indeed, the P-O peak is reported to be highly sensitive to the symmetry of the anion [39], [40], [52] which could potentially be perturbed by NH_3 adsorption on the NH_4^+ sites of NH_4PMo. Posttreatment is thought to desorb these NH_3 molecules. Indeed, samples without posttreatment or with moderate (50°C and 150°C) posttreatment temperatures fail to completely desorb NH_3, altering the P–O bond vibration. The intensity of the N–H peak decreases with higher

posttreatment temperatures, supporting this hypothesis. Additionally, the N–H/P–O ratio further substantiates this interpretation. In summary, posttreated samples exhibit crystallinity and solubility nearly to the reference, unlike pre-treated samples.

Among the posttreated samples, the one treated at 300°C most closely resembles the commercial NH_4PMo. This synthesis method will therefore be adopted: vacuum drying at 25°C overnight and under <30 mbar, followed by NH_3 flushing at 25°C and posttreatment at 300°C.

Phase 2: Supported Catalyst Development

In this section, H_3PMo was supported on two different materials: TiO_2 (P25, 50 m^2/g) and SiO_2 (FK320, 160 m^2/g). The HPMo loading (%ML) was varied on each support — a low loading (10% ML) and a high loading (70% ML) — to detect potential crystalline clusters of H_3PMo or NH_4PMo with the aim of discussing the dispersion of H_3PMo as a function of the loading/support and to compare catalyst performance based on loading and support type. The synthesis was performed via wet impregnation, followed by neutralization at 25°C and posttreatment at 300°C, aiming to obtain well-dispersed NH_4PMo.

Supported samples were also analyzed by IR and UV–Vis spectroscopy using the same protocol as in Phase 1 (p.39) (same Mo concentration for each sample solution) to compare their solubility with commercial NH_4PMo and H_3PMo.

Finally, the supports were compared based on their ability to neutralize the H_3PMo acidity, which can potentially reduce H_3PMo's propensity to be neutralized by NH_3. SiO_2 is considered relatively inert and acidic [53], while TiO_2 is amphoteric and interacts with H_3PMo [43], [46] [47]. Thus, SiO_2 is not expected to interact with H_3PMo as much as TiO_2.

From this point forward, the samples labeled "NH_4PMo-support" refer to the H_3PMo-support that underwent the optimal neutralization procedure discussed in the previous section. For simplicity, each sample received a specific name; Table 5 lists the abbreviations/code for the supported samples.

Table 5: List of abbreviations used for the samples.

Code	Samples on TiO_2	Code	Samples on SiO_2
TH10	H_3PMo-TiO_2 10%ML	SH10	H_3PMo-SiO_2 10%ML
TH70	H_3PMo-TiO_2 70%ML	SH70	H_3PMo-SiO_2 70%ML
TN10	NH_4PMo-TiO_2 10%ML	SN10	NH_4PMo-SiO_2 10%ML
TN70	NH_4PMo-TiO_2 70%ML	SN70	NH_4PMo-SiO_2 70%ML

Results

Infrared spectroscopy

The graphs show characteristic peaks of $PMo_{12}O_{40}^{3-}$ only for samples with high loadings (70% ML) (Figure 15 and 16), but the vibrations peaks from the supports overlap most of the peaks of $PMo_{12}O_{40}^{3-}$ (Figure B and C in appendices).

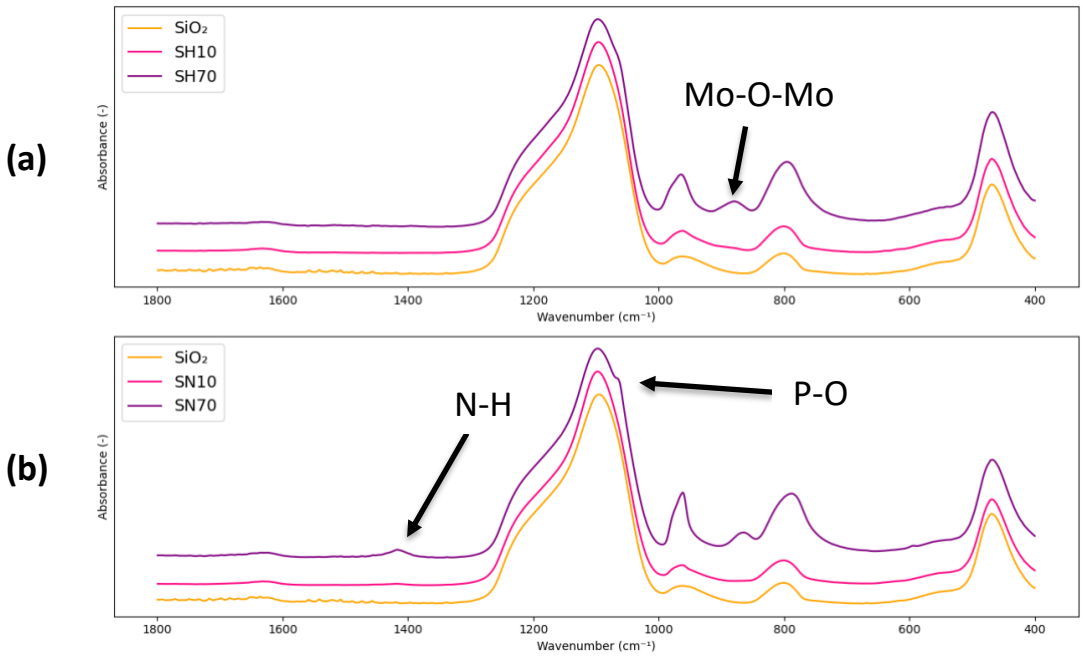

Figure 15: Infrared spectra of SiO_2-supported: (a) H_3PMo/SiO_2, (b) NH_4PMo/SiO_2.

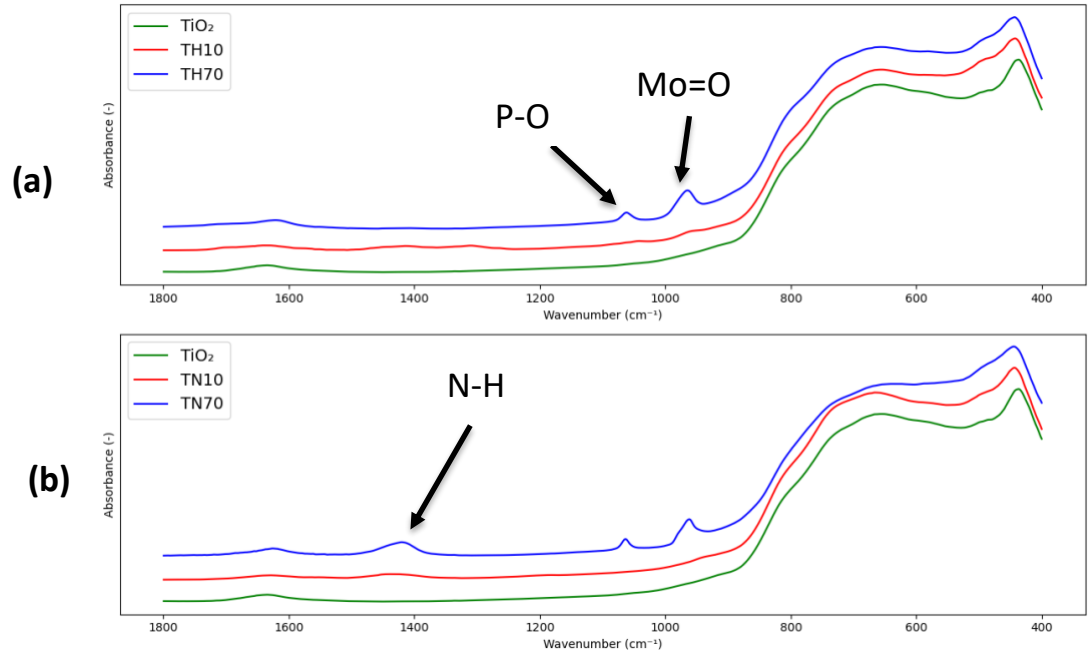

Figure 16: Infrared spectra of SiO_2-supported: (a) H_3PMo/SiO_2, (b) NH_4PMo/SiO_2.

UV-Vis spectroscopy

UV analyses reveal signals comparable to the commercial bulk versions for both supports (Figure 17). Neutralized samples exhibit lower solubility than their acidic counterparts. The neutralized versions resemble to the commercial NH_4PMo signal, although a distinct peak remains at 275 nm.

TPD-NH_3

The impregnated samples on the supports are compared to pure H_3PMo in its acidic form and to their respective supports (Figure 18). The acidic H_3PMo exhibits two acid sites: a weaker site around 160°C and a stronger site at 450°C. When supported on SiO_2 (Figure 18a), the stronger acid site is no longer visible. At high loading (70%ML), the peak extends to higher temperatures. The two peaks represent a combination of the acid sites from the support and H_3PMo. A similar behaviour is observed for samples supported on TiO_2 (Figure 18b).

However, pure TiO_2 shows stronger acid sites than SiO_2 (200–400°C for TiO_2 vs. 100–200°C for SiO_2).

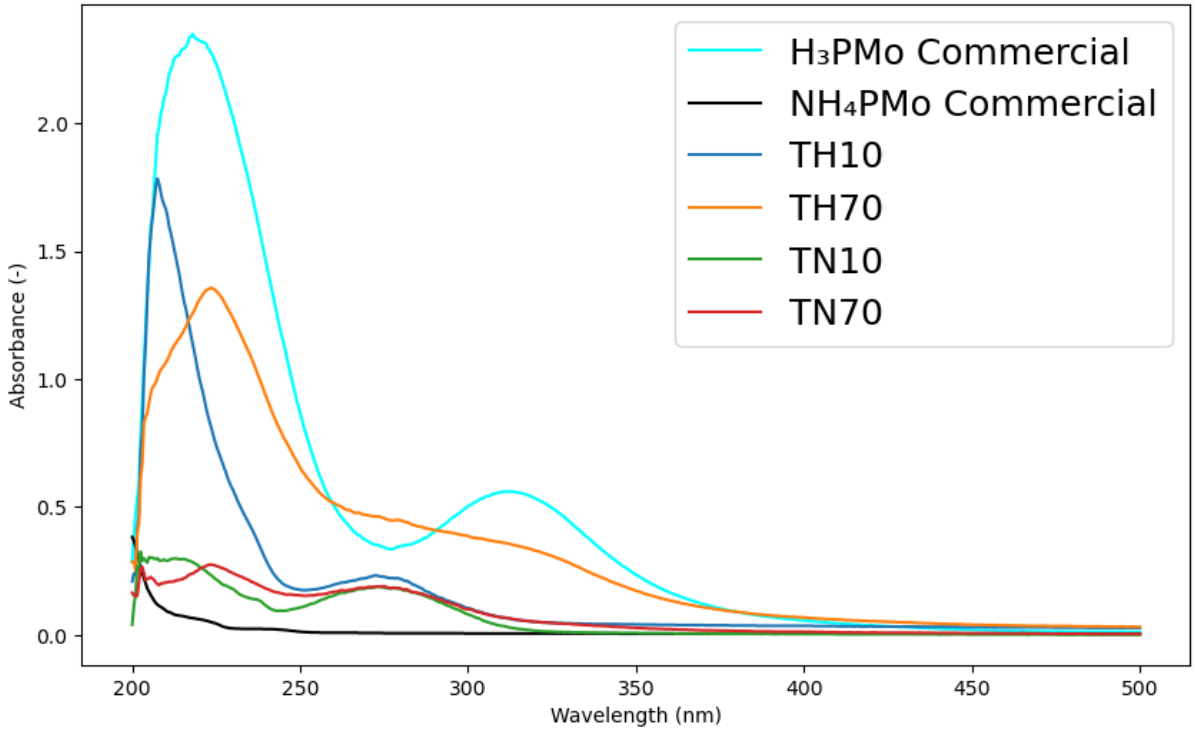

(a)

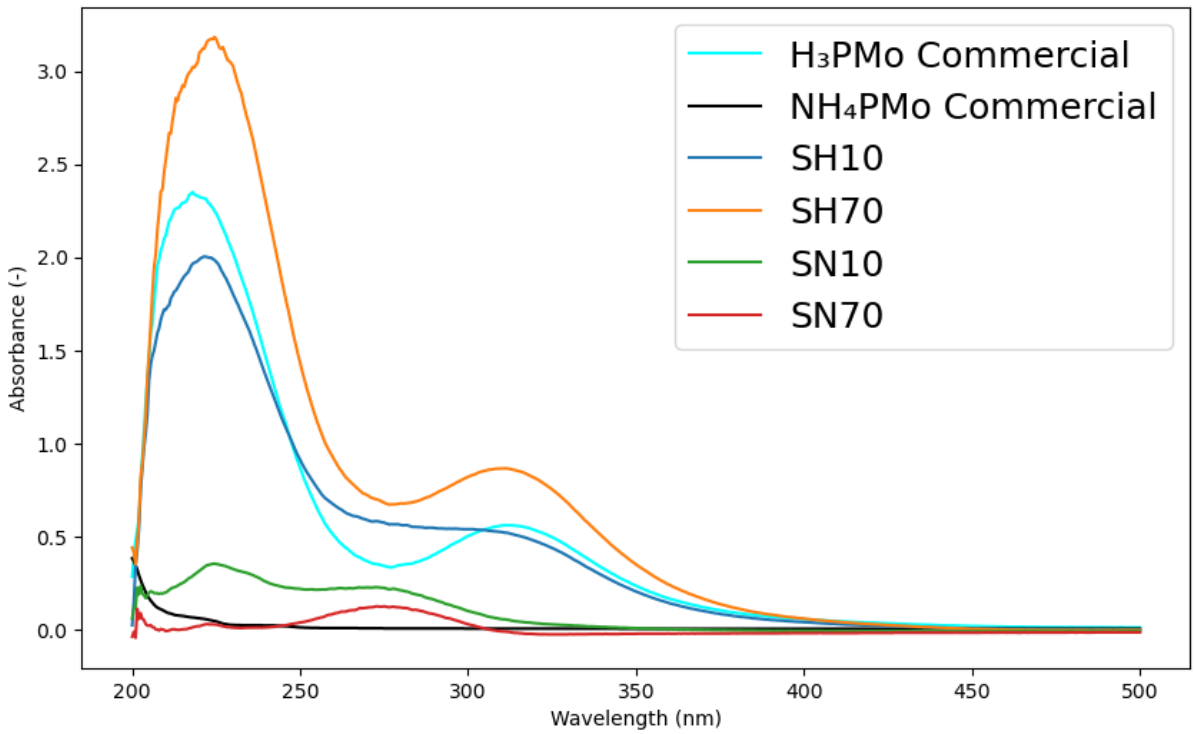

(b)

Figure 17: UV spectra of H_3PMo- and NH_4PMo-supported on (a) TiO_2 and (b) SiO_2 in ethanol solution (filtered solutions at equivalent concentrations).

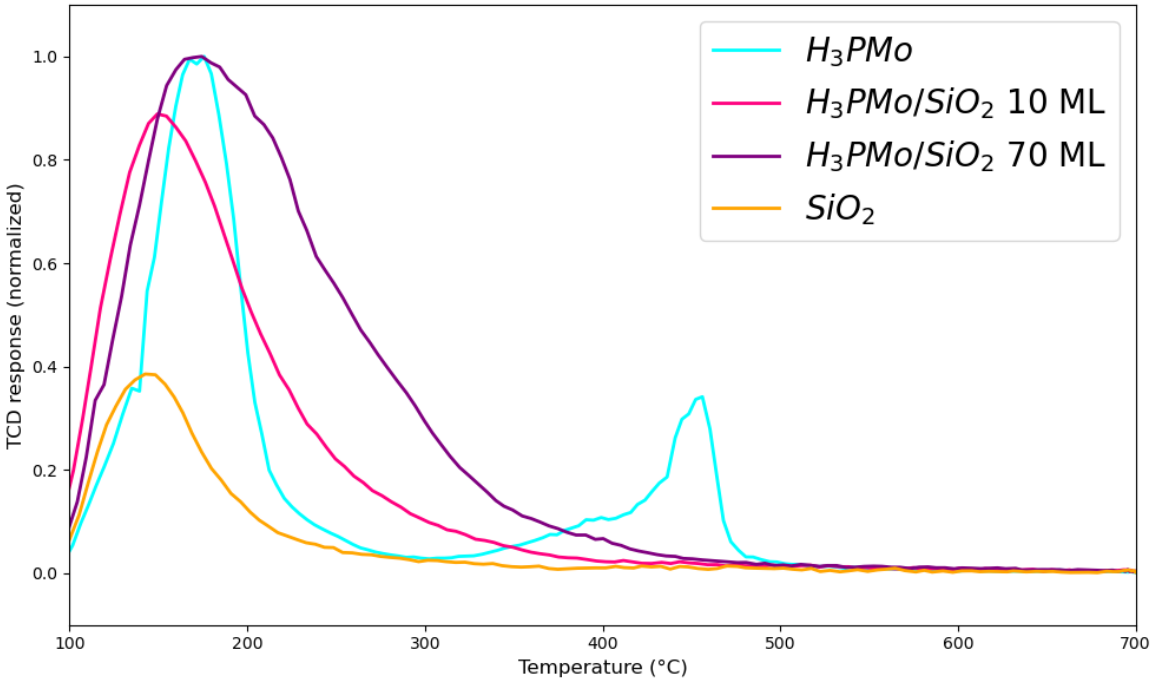

(a)

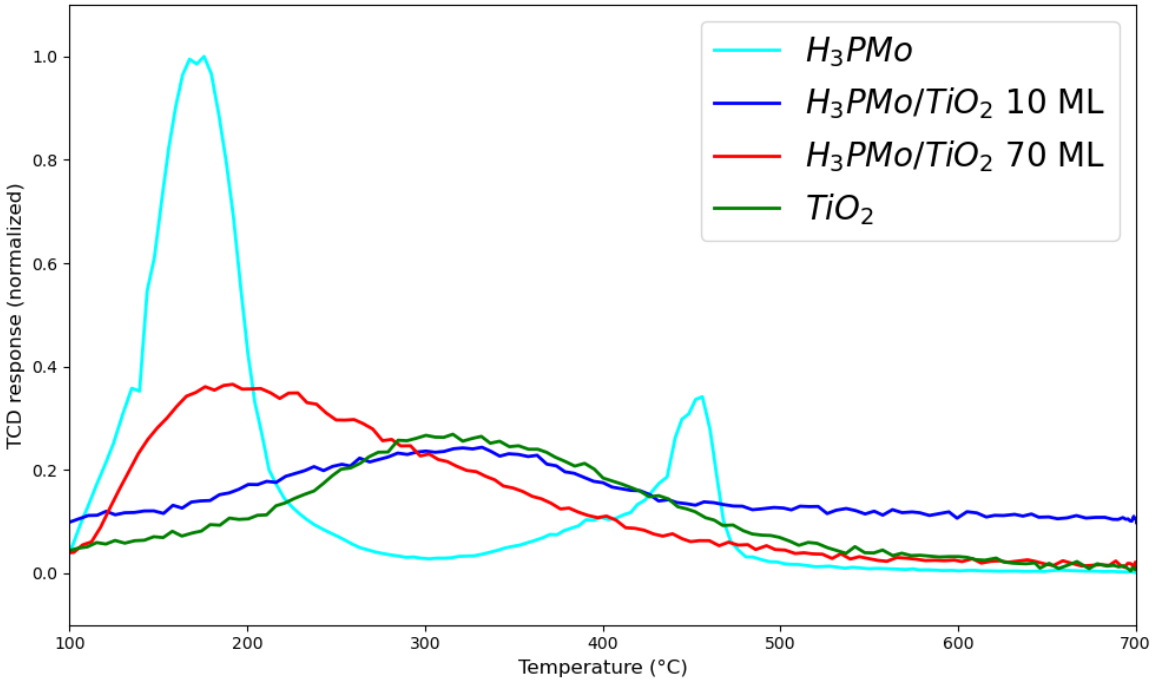

(b)

Figure 18: TPD-NH_3 profiles of supported H_3PMo: (a) on SiO_2, (b) on TiO_2.

PXRD

PXRD patterns of H_3PMo, NH_4PMo and their supported versions are shown in Figure 19. H_3PMo/TiO_2 diffractograms (10 and 70 ML%) show only peaks coming from TiO_2 and no peak owing to H_3PMo was visible (Figure 19). NH_4PMo/TiO_2 diffractograms (10 and 70 ML%) show only peaks coming from TiO_2 as well.

In contrast, H_3PMo/SiO_2 (70 ML%) showed peaks at 7° and 28° corresponding to commercial H_3PMo while H_3PMo/SiO_2 (10 ML%) did not show any peak. Some characteristic peaks of commercial NH_4PMo at 11° and 26° are observed for NH_4PMo/SiO_2 for 70 ML% only (Figure 19). The same peak at 22° is also observed for both H_3PMo/SiO_2 (70 ML%) and NH_4PMo/SiO_2 (70 ML%).

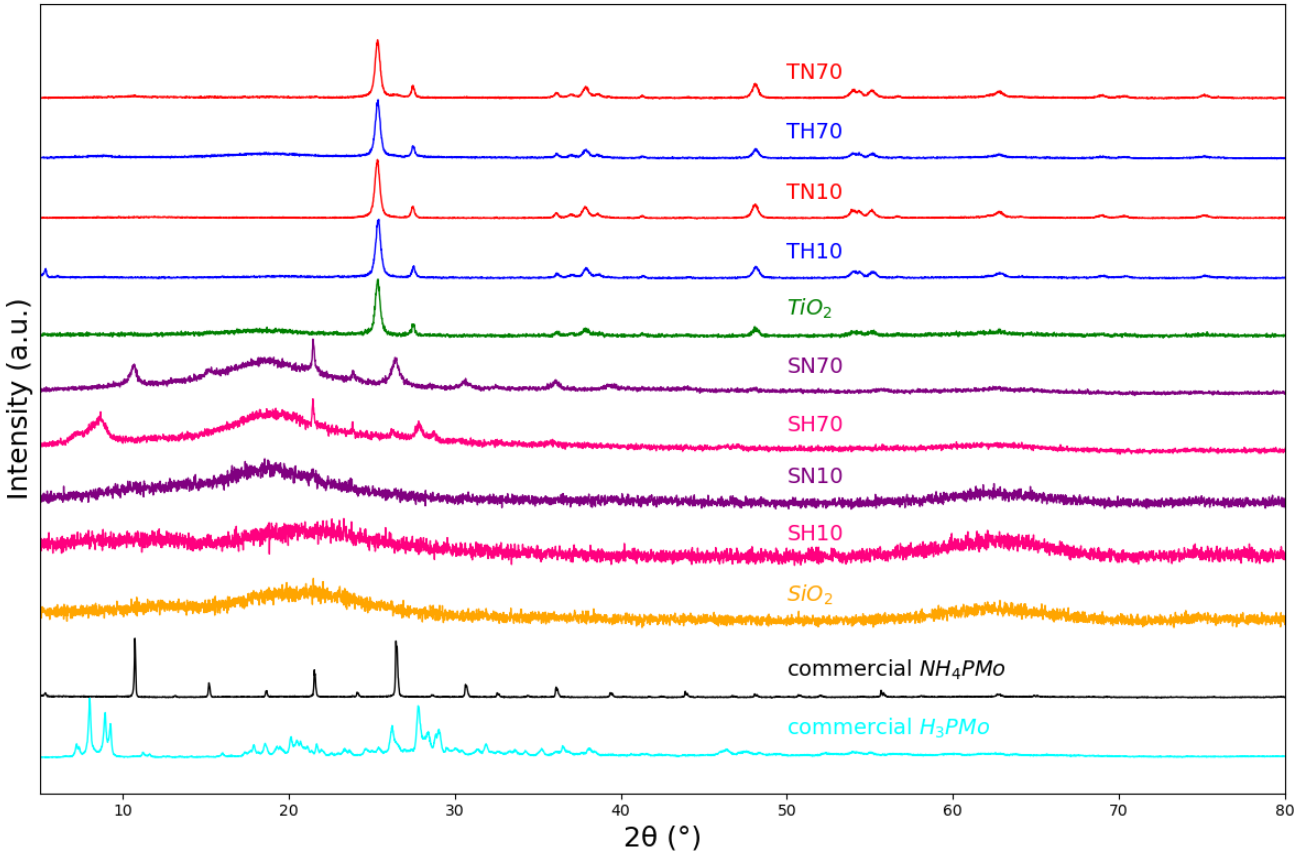

Figure 19: PXRD diffractograms of supported and/or neutralized samples compared to their respective supports and commercial references.

Discussion

The supports appear to pre-neutralize the strong acid sites of H_3PMo, which are no longer detected upon supporting. The peaks of the supported samples in TPD-NH_3 broaden as the loading increases for both supports. A plausible explanation could be that there is a higher likelihood of H_3PMo aggregation or overlap, leading to sites that are not in direct contact with the support. Furthermore, it can be assumed that all the high-potential interaction sites for H_3PMo on the support were occupied by the first molecules, leaving weaker interactions with the support for the remaining H_3PMo molecules, thereby protecting their strong acidic sites from neutralization by the support. Another key observation is that most NH_3 on the supported samples desorb below 300°C, which could raise some concerns about the stability of NH_4PMo-supported samples (after NH_3-flush) during posttreatment following neutralization.

However, the measured NH_3 desorption temperature cannot rigorously be compared with the posttreatment temperature, as the TPD-NH_3 analysis involves an unavoidable drying step at 300°C before adsorption (while this is not the case during the synthesis). This could potentially alter the nature of the sample. Indeed, harsh drying steps are known to reduce H_3PMo and therefore, its acid strength.

TiO_2 exhibits predominantly stronger acid sites compared to SiO_2, which is noteworthy. SiO_2 is typically regarded as an acidic support with an isoelectric point of 2, whereas TiO_2 is amphoteric with an isoelectric point around 6 [53]. The main reason is that SiO_2 has a low density of silanol groups (Si–OH), which are the strong acid sites responsible for its low isoelectric point but may not be detectable via TPD-NH_3. TiO_2 effectively neutralizes H_3PMo and achieves good

dispersion even at 70%ML, consistent with previous literature [43], [46] [47] [47]. Conversely, H_3PMo appears to form crystalline agglomerates at high loadings when supported on SiO_2. These agglomerates match the reference patterns for both H_3PMo/SiO_2 (before neutralization) and NH_4PMo/SiO_2 (after neutralization). This suggests that neutralization by NH_3 transforms H_3PMo to into NH_4PMo at SiO_2' surface.

In summary, (1) H_3PMo is neutralized by both supports and exhibits a higher number of acidic sites at high loadings. (2) Samples supported on TiO_2 show no evidence of crystalline phase (at the exception of TiO_2 itself) regardless of the loading, suggesting potentially good dispersion of H_3PMo on this support. In contrast, H_3PMo/SiO_2 at 70% ML exhibits crystals with a crystalline phase resembling that of NH_4PMo when neutralized by NH_3. (3) This, along with the presence of the N-H vibration peak in the IR spectra for supported samples neutralized by NH_3 at high loading, suggest that the synthesis of well-dispersed NH_4PMo onto SiO_2 and TiO_2 was successful. However, at this stage, it remains difficult to confirm this definitively. But XPS or ICP-AES analyses could provide more information and confirm or not the synthesis of well-dispersed NH_4PMo on a support.

Phase 3.1: Catalytic tests

In this section, all synthesized supported samples were tested for 18 hours at 210°C to compare them with the commercial bulk catalysts H_3PMo and NH_4PMo. The catalyst amount was fixed at 5 mol% of Mo relative to 1,2-hexanediol for each test. A blank test (no catalyst) and tests using only the supports were also conducted to determine their activity under these conditions. In this case, the added amount matches the support mass used with H_3PMo /support 10%ML, as this is the maximum support mass among the samples being evaluated.

Results

Commercial H_3PMo has achieved higher conversion and selectivity than NH_4PMo under these conditions (Figure 20). TiO_2-supported samples have outperformed SiO_2-based catalysts. Different loadings (the nature of the support being kept) exhibited similar activity, with no significant differences. This trend holds when comparing acidic (H_3PMo /support) to neutralized (NH_4PMo/support) catalysts.

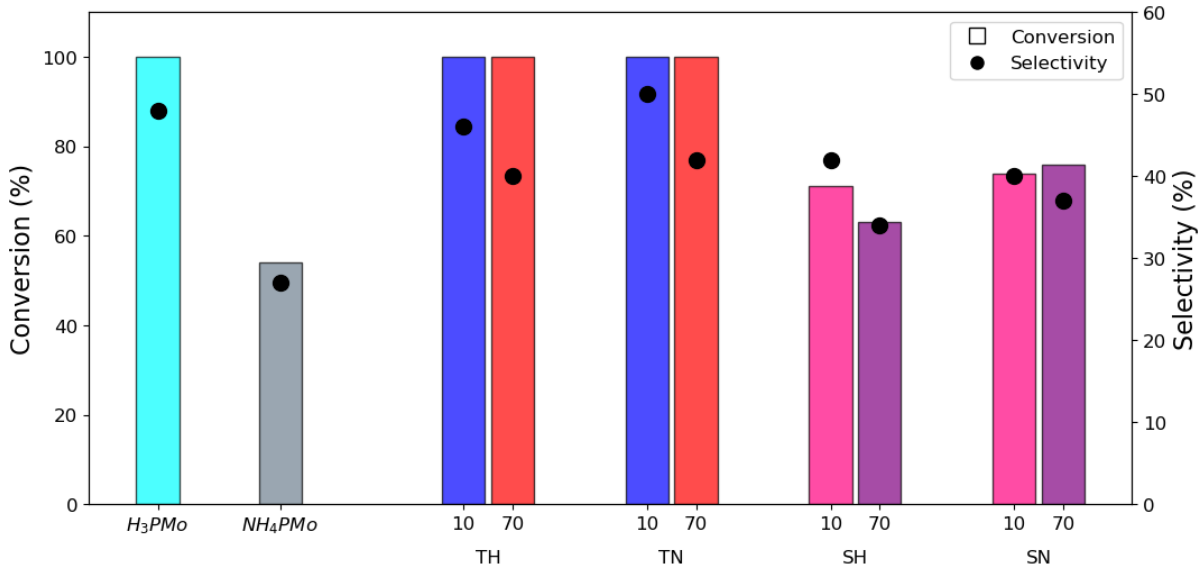

Figure 20: Catalytic performances of H_3PMo, NH_4PMo, H_3PMo/TiO_2, NH_4PMo/TiO_2, H_3PMo/SiO_2 and NH_4PMo/SiO_2 at 10 or 70ML%. Reaction conditions: 5% mol Mo, 18 h, 210°C.

The blank test shows a 3% conversion without any catalyst (Figure 21). The presence of SiO_2 slightly increases this conversion, but pure TiO_2 alone yields a notably high conversion (55%) with low selectivity. In contrast, both the blank and SiO_2 exhibit relatively high selectivity, exceeding 40%.

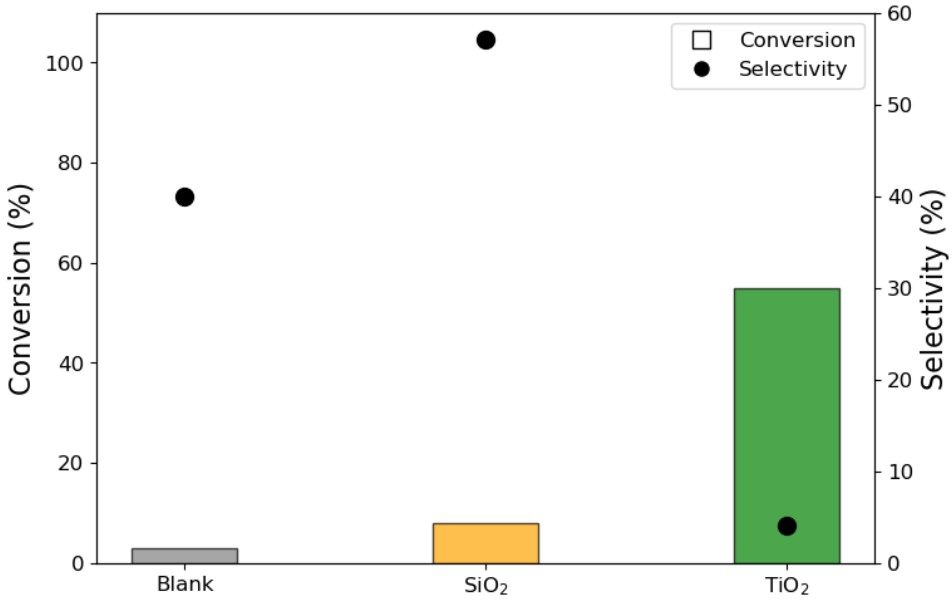

Figure 21: Catalytic performances of blank, pure SiO_2, and pure TiO_2. Reaction conditions: 5% mol Mo, 18 h, 210°C.

Discussion

The results for the commercial bulk samples do not match those in Figure 6 from the Strategy section (p.24). Indeed, H_3PMo shows higher selectivity, whereas NH_4PMo exhibits lower conversion and selectivity, even though the same samples were used. This discrepancy may be due to differences in catalyst mass at the start of each test. The tests shown in Figure 6 used 15 mg of catalyst, corresponding to slightly under 15% Mo (in mol Mo/1,2-hexanediol), whereas the tests reported here used 5% Mo. This difference could explain the variation in results and reversal of trends. With H_3PMo at or above 15% Mo, it may

activate secondary reactions involving 1-hexene. This remains hypothetical and is not further examined here as it falls out of the scope of this study.

The high conversion of TiO_2-supported samples (Figure 20) likely arises from the high baseline conversion of TiO_2 alone. One hypothesis is that TiO_2's amphoteric nature [53] and its higher number of acidic sites, as shown in TPD-NH_3, facilitate the adsorption of reactants. This, in turn, promotes the desired reaction. This explanation aligns with TiO_2's elevated conversion shown in Figure 18, where reactants seem more adsorbed than truly converted, accounting for the low selectivity only for TiO_2 only. In contrast, SiO_2 is more inert [54] and adsorbs less, resulting in lower conversion. Given the high selectivity observed for low conversion in a catalyst-free test (blank), the high selectivity of SiO_2 is not surprising. No significant differences appear between loadings (10%ML vs. 70%ML) or cation types (H^+ vs. NH_4^+). Leaching may play a role, but if we compare to the bulk references, NH_4PMo-supported samples would be expected to show lower conversion and selectivity than their acidic counterparts as the latter are highly soluble without support. A possible hypothesis is that H_3PMo is always neutralized in each sample, either by the support alone (H_3PMo /supported) or by both the support and NH_3 (NH_4PMo/supported). Being neutralized in each case, it provides the similar catalytic activity.

Phase 3.2: Recycling

In this section, the commercial bulk catalysts are recycled to demonstrate that the insolubility of NH_4PMo enables its recovery and reuse, unlike H_3PMo. In addition, all samples are recycled 4 times (each time 5% mol. of Mo, 5h, 210°C, unless otherwise specified) to potentially demonstrate stable activity over repeated cycles. Because unavoidable mechanical losses of catalyst occur between each recycling step, the reaction volume is adjusted to the recovered catalyst mass to maintain a 5% mol ratio of Mo to 1,2-hexanediol. This procedure assumes that the mechanically lost mass is homogeneous and includes both the support and the active phase.

The samples are also characterized by IR (FTIR in the transmittance mode and ATR). Samples labeled with an “R” preceding their abbreviation denote catalysts that have been recycled once.

Results

Recycling tests

The bulk catalysts were recycled once and the Mo charge was 20% mol. for simplicity in mass measurements, with a 4-hour reaction time (Figure 22).

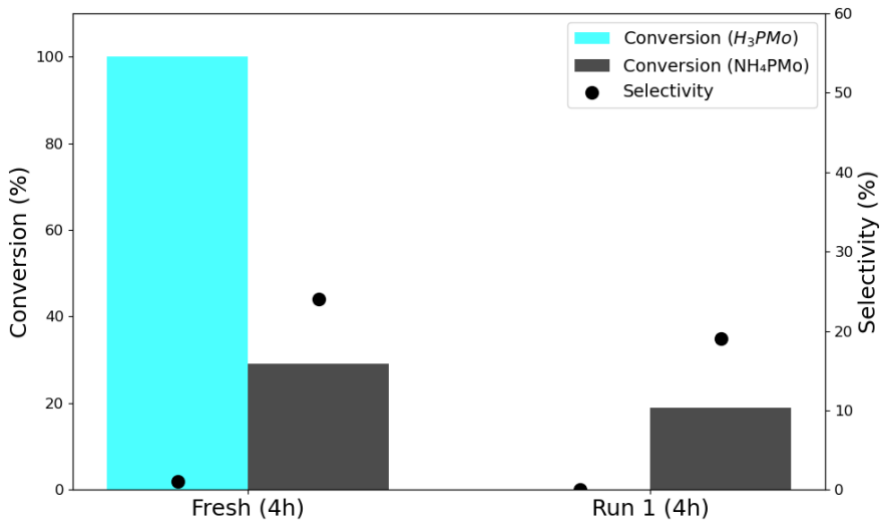

Figure 22: Results of recycled bulk H_3PMo and NH_4PMo catalysts (20% Mo, 4 h, 210°C).

A key observation is that H_3PMo cannot be recycled, whereas NH_4PMo retains its activity after recycling. H_3PMo achieved 100% conversion but with extremely low selectivity (1%) while NH_4PMo showed a lower conversion (25%) but a higher selectivity (24%). A slight conversion and selectivity decrease was observed after one recycling. As previously mentioned, the results depend on the engaged catalyst amount and will not be further discussed in this document.

Recycling H_3PMo /TiO_2 and NH_4PMo/TiO_2 leads to higher selectivity and conversion in the first reuse step (Figure 23). After that, both catalysts maintain stable performance across multiple cycles, consistently reaching nearly 100% conversion. A difference in activity is observed between the low (10%ML) and high (70%ML) loadings during their first use, but no significant difference emerges between the acidic (H^+) and neutralized (NH_4^+) versions.

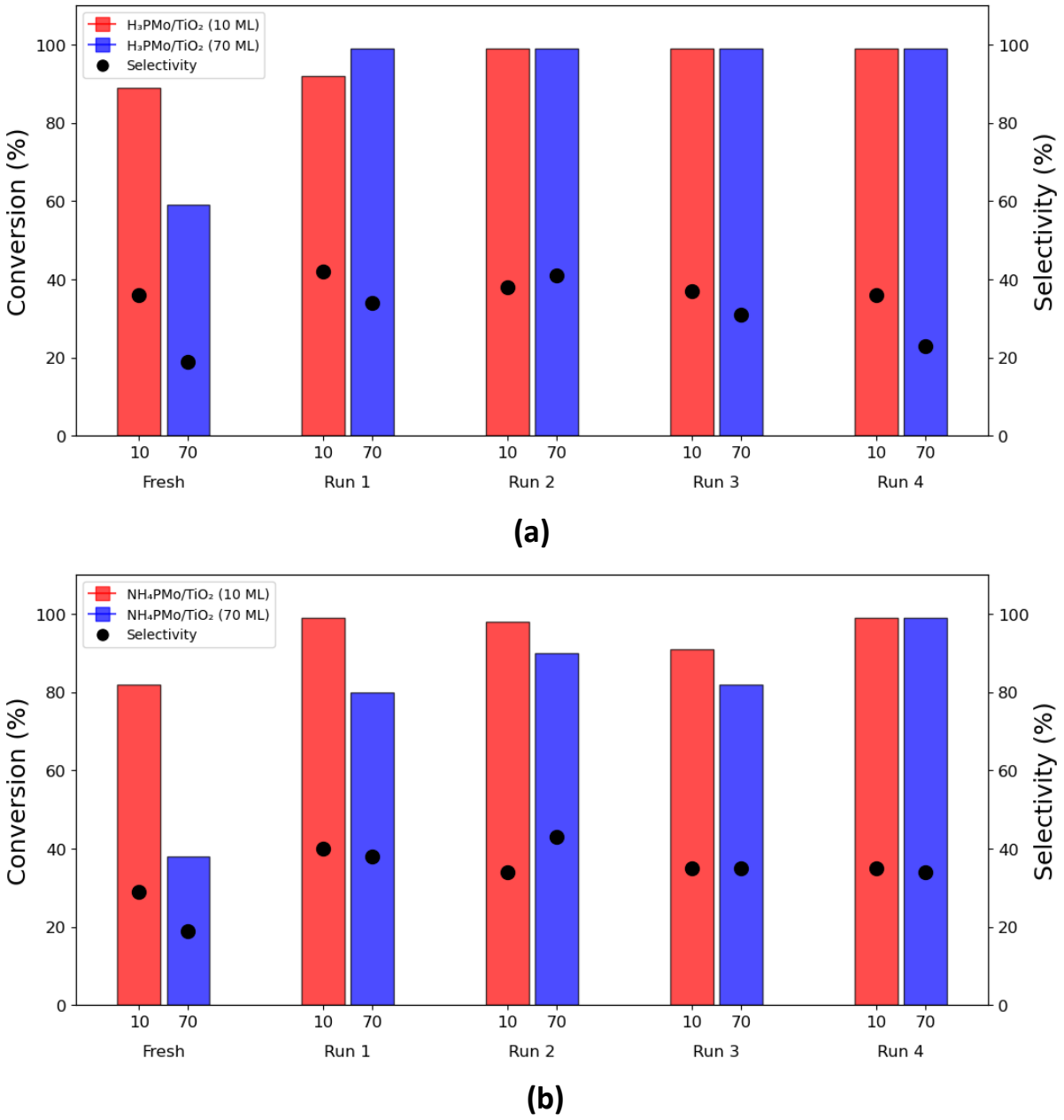

Figure 23: Recycling performance of (a) H_3PMo/TiO_2 10ML and 70ML (b) NH_4PMo/TiO_2 10ML and 70ML (5%Mo, 5h, 210°C).

H_3PMo /SiO_2 could only be recycled three times due to excessive mechanical losses (Figure 24a). Its performances improved between each use except for sample SH70 at the second recycle (Run 2), which showed selectivity drop. NH_4PMo/SiO_2 delivered similar results but lost selectivity starting at the third recycle (Run 3) (Figure 24b).

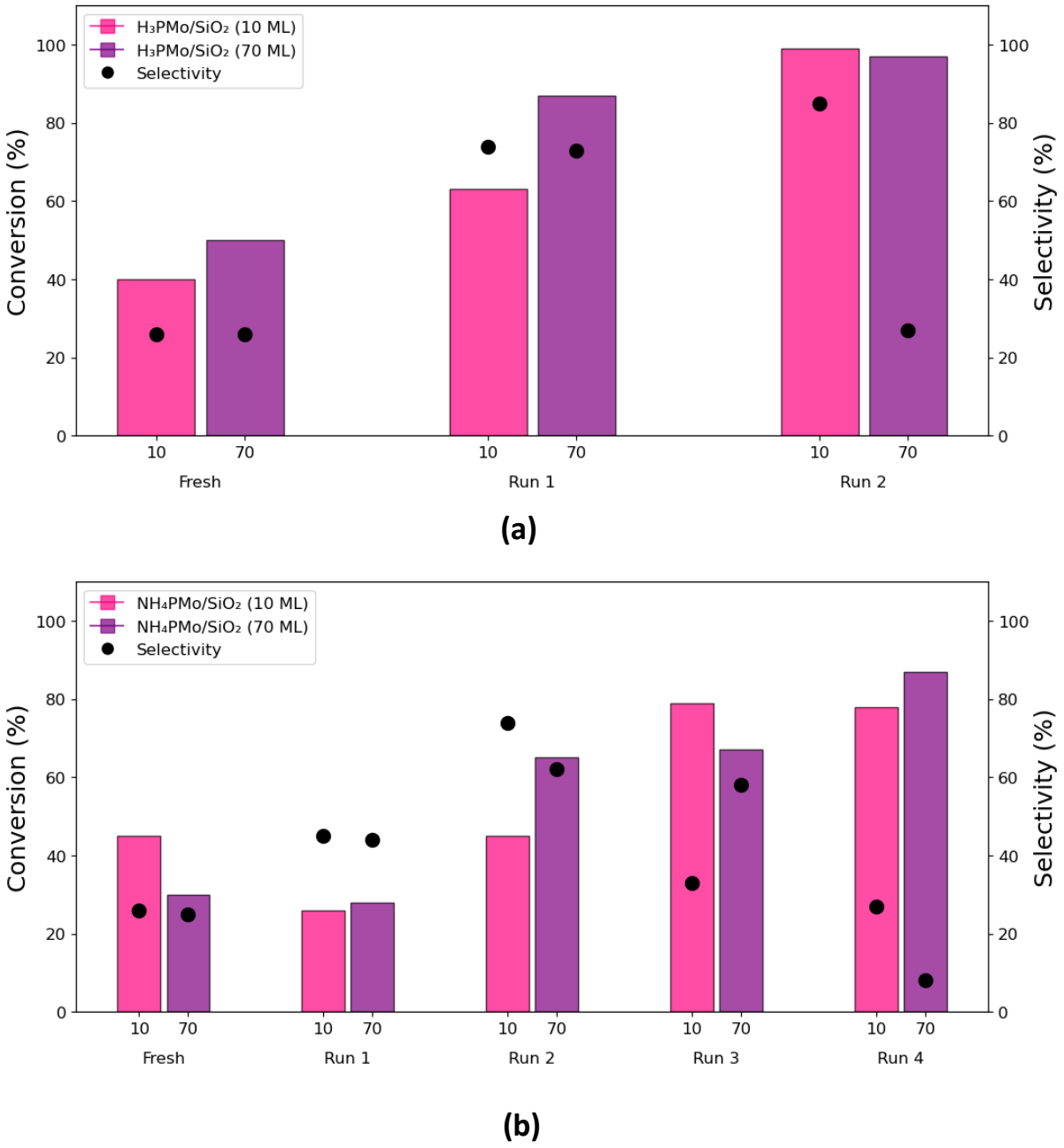

Figure 24: Recycling performance of (a) H_3PMo/SiO_2 10ML and 70ML (b) NH_4PMo/SiO_2 10ML and 70ML (5%Mo, 5h, 210°C).

Infrared spectroscopy

The IR spectrum of recycled commercial NH_4PMo was analyzed by FTIR (instead of ATR) to enhance the signal (Figure 25). It displays the same features as the fresh sample, except for a CO_2 vibration peak and a C–H vibration peak [55].

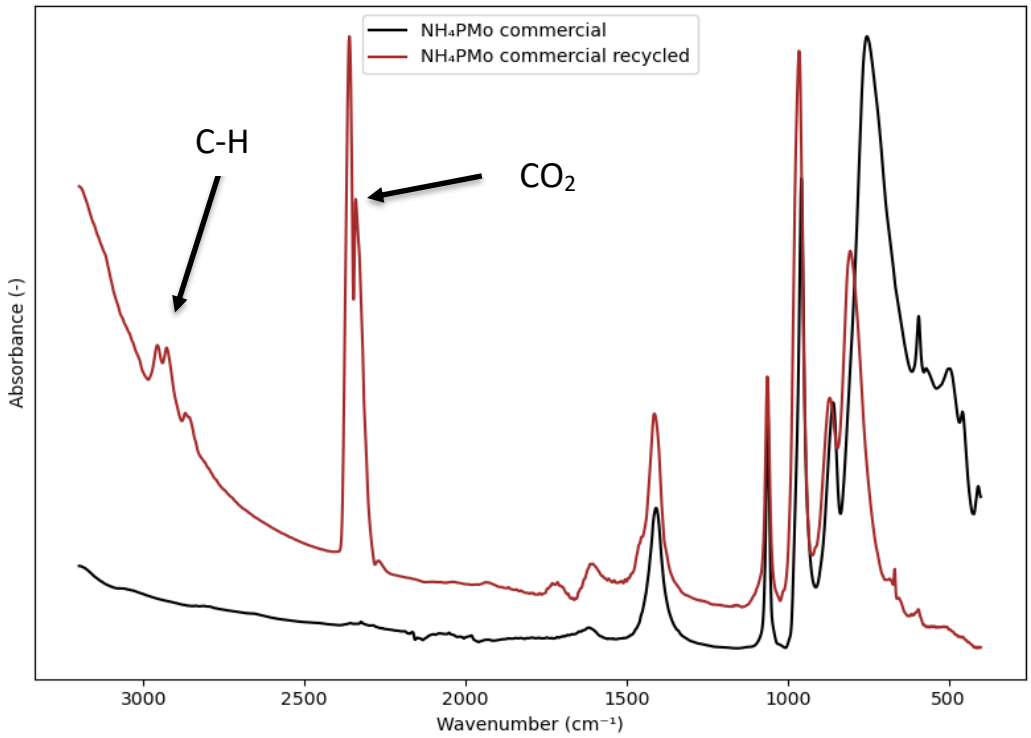

Figure 25: Infrared spectra comparing fresh and recycled commercial NH_4PMo.

SiO_2-supported samples lose the characteristic peaks of $PMo_{12}O_{40}^{3-}$ after recycling (Figure 26). This behavior is also observed in TiO_2-supported samples (Figure 27). Before recycling, only the high-loading (70%ML) samples display the characteristic N–H, P–O, or Mo–O vibration peaks.

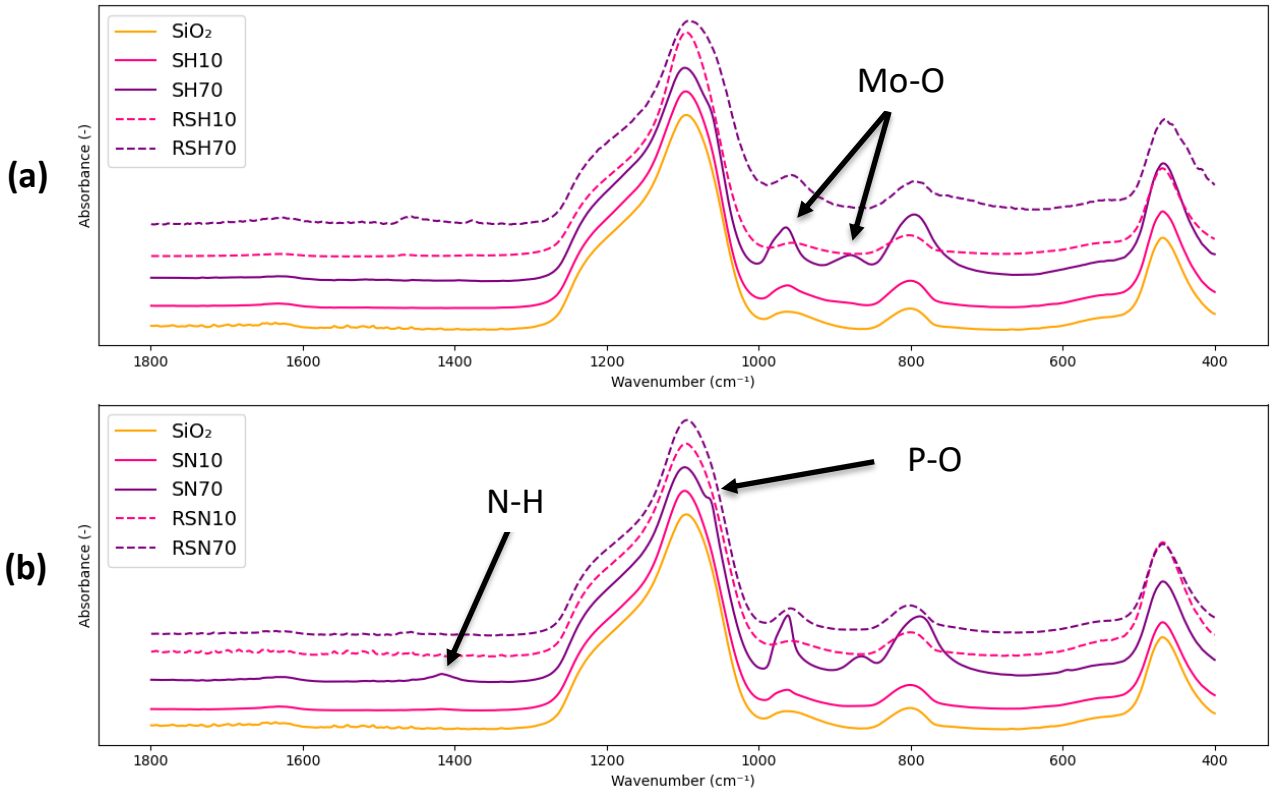

Figure 26: Infrared spectra of SiO_2-supported and recycled samples: (a) $H_3PMo–SiO_2$, (b) $NH_4PMo–SiO_2$.

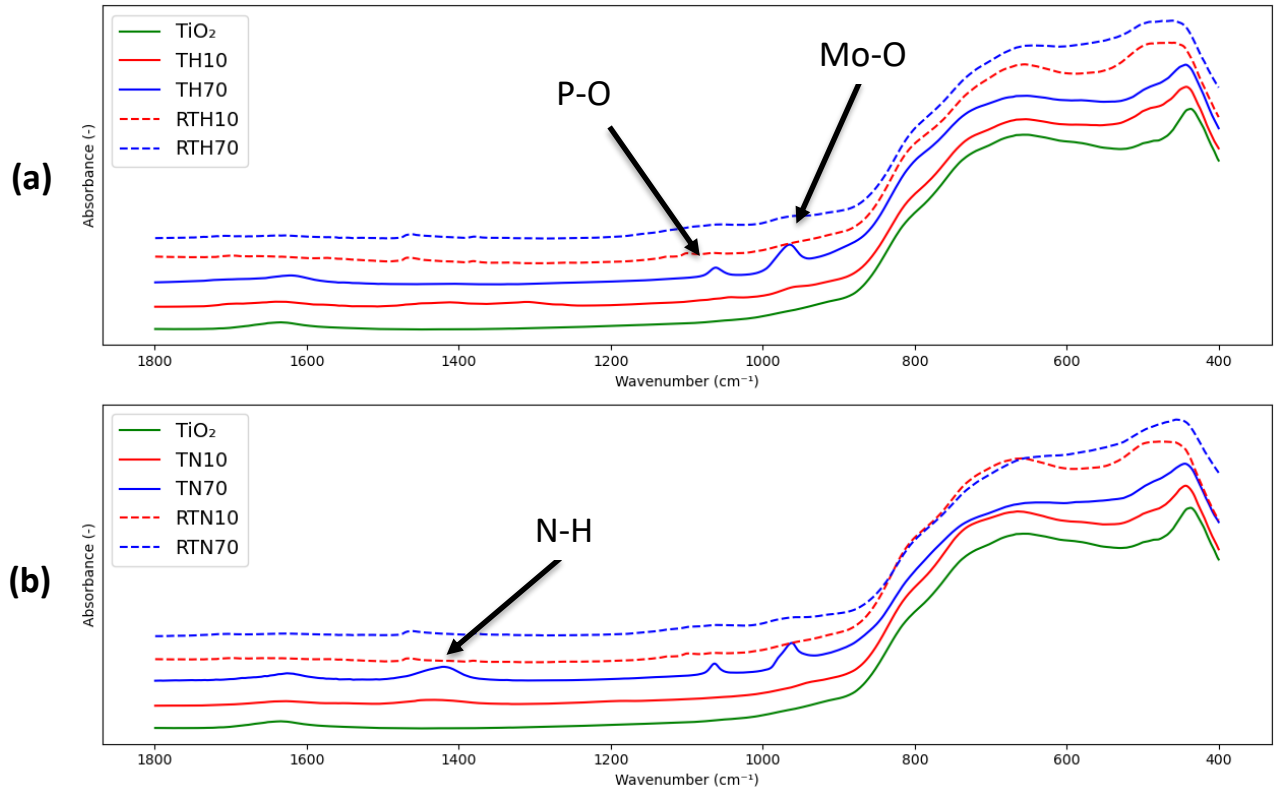

Figure 27: Infrared spectra of TiO_2-supported and recycled samples: (a) $H_3PMo–TiO_2$, (b) $NH_4PMo–TiO_2$.

Discussion

Results in Figure 19 indicate that the total amount of bulk catalyst added affects selectivity. H_3PMo may participate in secondary reactions with the desired product, explaining the very low selectivity when using more than 20% Mo. Commercial NH_4PMo confirms its recyclability, unlike H_3PMo. However, when supported, both catalysts show increasing activity with each recycle. An initial explanation was a possible contamination from residual product, yet this does not clarify the concurrent rise in conversion. Adjusting the reaction volume for each reuse could also introduce errors in weighing or pipetting. Consequently, these results are not straightforward to interpret. IR spectra prove that the Keggin structure remains intact after recycling, though it is challenging to detect in supported samples at low loading.

The key conclusions are: (1) commercial bulk NH_4PMo is recyclable, whereas bulk H_3PMo is not; (2) the tested supported catalysts retain activity through four recycles; (3) evidence of the Keggin structure persists after recycling; and (4) TiO_2-supported catalysts exhibit significantly higher conversion than those on SiO_2, likely because it adsorbs significantly more reactants, facilitating the desired reaction.

Phase 3.3: Leaching study

Cold filtration tests were performed on all samples to evaluate potential leaching. After five hours of catalytic testing (5% mol. Mo, 210°C), the solutions were cold (0°C) filtered to remove the solid catalyst. Then, the filtered solutions were reheated to 210°C and tested for another 5 hours. Each solution was analyzed twice — before filtration (BF) and after filtration (AF) — to determine whether the DODH-activity continues in the absence of the solid catalyst.

Results

Cold filtration tests

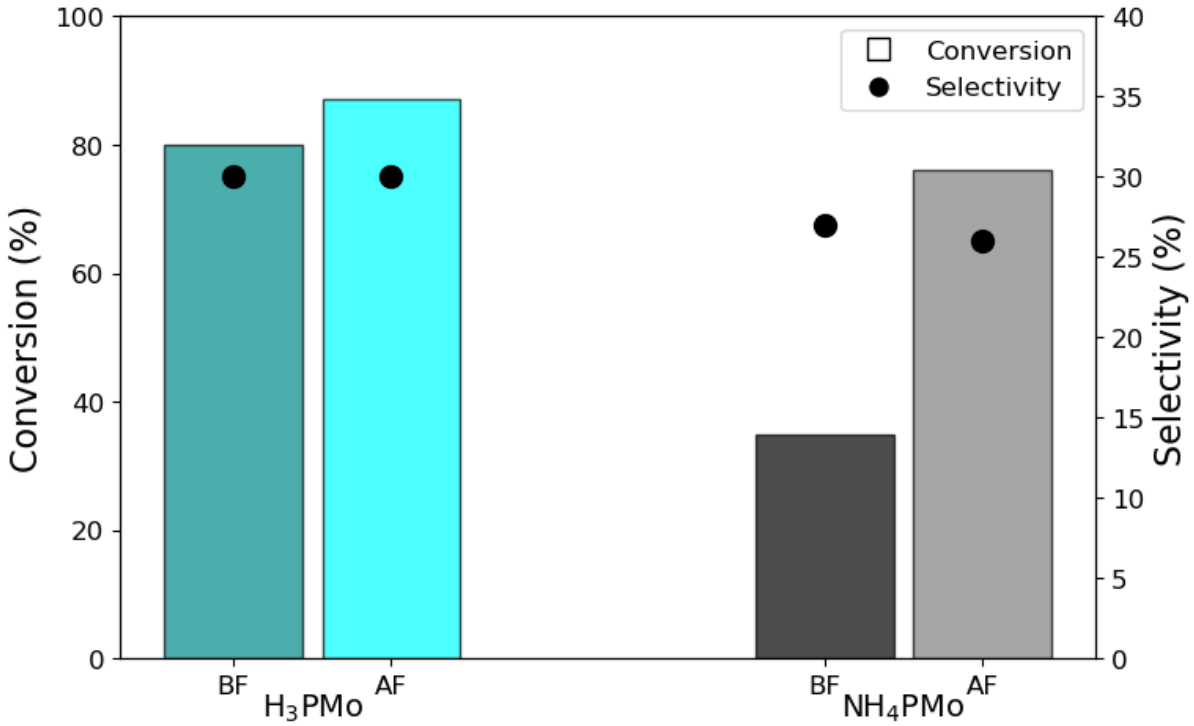

Figure 28: Cold filtration test of commercial bulk H_3PMo and NH_4PMo samples (BF = before filtration, AF = after filtration).

Both commercial bulk catalysts, H_3PMo and NH_4PMo, show an increase in conversion after filtration (Figure 28). NH_4PMo exhibits a larger rise, on the order of 40%.

It is clear that TiO_2-supported samples (Figure 29) exhibit a smaller increase in conversion after filtration compared to those on SiO_2 (Figure 30). Although both supports show higher activity after filtration, the effect is less pronounced for TiO_2 than for SiO_2.

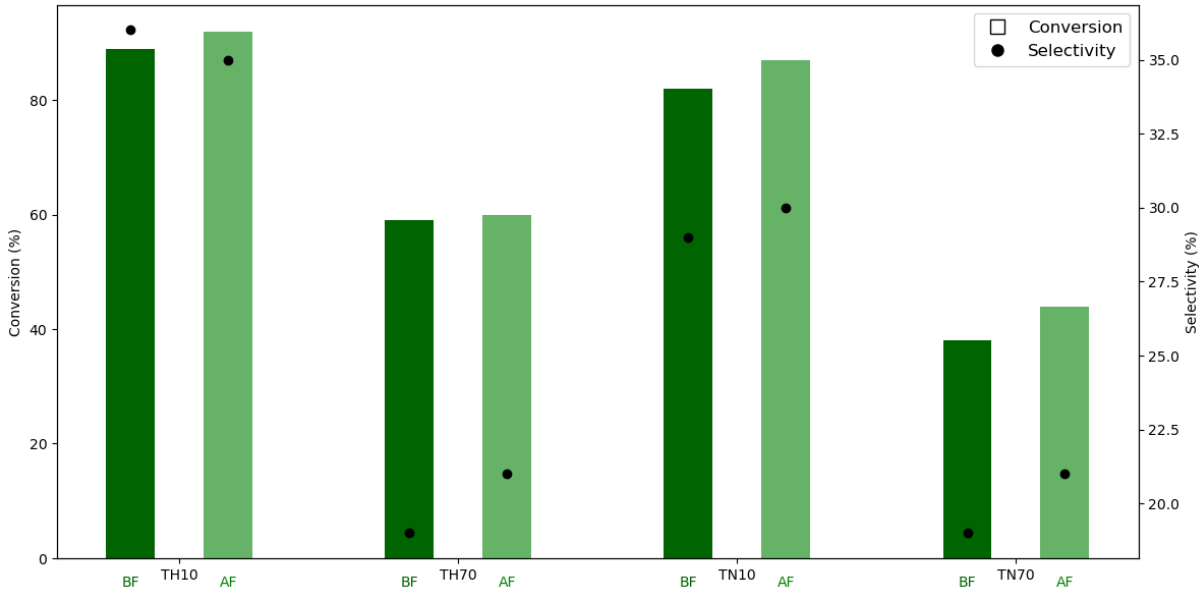

Figure 29: Cold filtration test of H_3PMo-TiO_2 and NH_4PMo-TiO_2 samples (BF = before filtration, AF = after filtration).

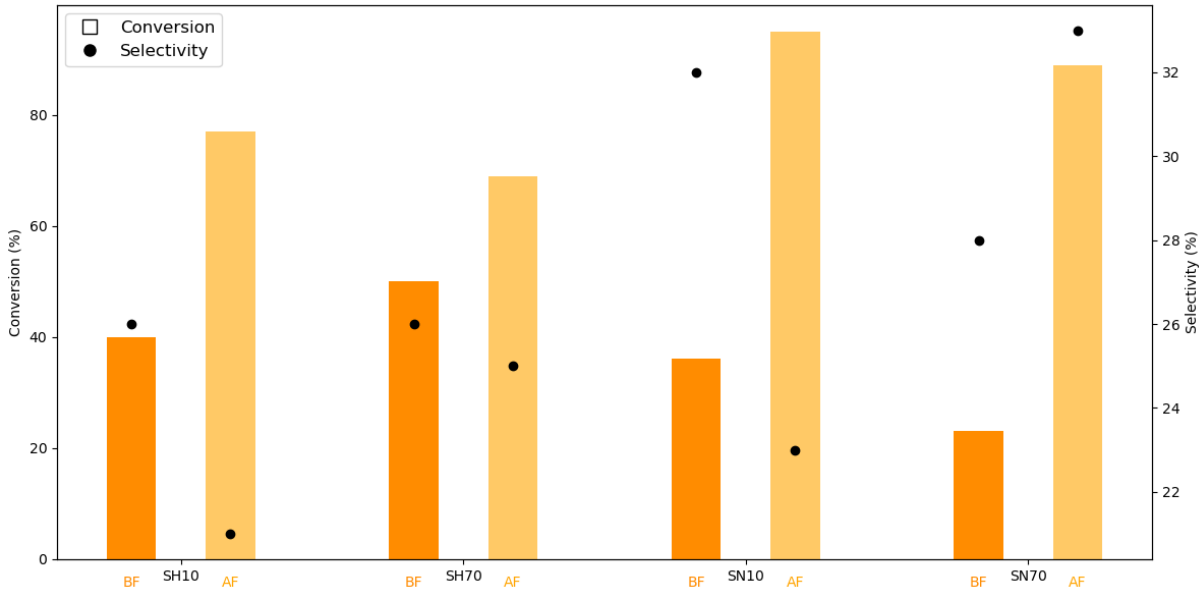

Figure 30: Cold filtration test of H_3PMo-SiO_2 and NH_4PMo-SiO_2 samples (BF = before filtration, AF = after filtration).

Discussion

The bulk (H_3PMo and NH_4PMo) and their SiO_2-supported versions all exhibited significant activity after filtration, evidencing the occurrence of leaching. In the case of TiO_2-supported catalysts, it was difficult to confirm whether leaching occured (except for TH70 and TN70), as the tests conducted before filtration achieve conversions close to 100%. To clarify, the same experiment should be repeated over a shorter timeframe to observe any potential increase in conversion. Conversely, TH70 and TN70 show no significant activity, even while in the so-called kinetic regime (before reaching a stable conversion close to 100% in this case). These results do not entirely align with the UV findings, which indicate lower solubility for the samples neutralized by NH_3. One would have expected an almost negligible increase in conversion for all SN samples, as UV spectroscopy evidenced less leaching in ethanol. Several possible explanations remain: (1) solubility conditions differ in ethanol or 3-octanol, (2) TiO_2 may retain H_3PMo more effectively due to its neutralization capabilities, unlike the more inert SiO_2, which releases $PMo_{12}O_{40}^{3-}$ more readily regardless of the cation.

An uncertainty remains regarding the nature of the active phase during the reaction. It is certain that there is a homogeneous contribution from the catalysts, as evidenced by the cold filtration tests on the bulk samples, but it is challenging to determine whether the solid phase is active or not.

Conclusion

The synthesis with a posttreatment at 300°C shows the closest resemblance to commercial NH_4PMo in terms of solubility, IR vibrational peaks and secondary structure (as evidence by PXRD). Specifically, the P-O peak, which is sensitive to the symmetry of the anion, sharpens as the post-treatment temperature increases. The suggested hypothesis is that the NH_4^+ cations adsorb excess NH_3, which modifies the P-O bond vibration. This excess NH_3 would desorb completely at 300°C.

Despite a significant indication in PXRD revealing the same crystalline phase as NH_4PMo for the SN70 sample, it is difficult to confirm that all supported catalysts have been fully neutralized by NH_3. Furthermore, TPD-NH_3 analyses show that both supports partially neutralize H_3PMo and that most of the NH_3 desorbs before 300°C. This observation should be taken into account, though cautiously, when considering the implications of the 300°C posttreatment. However, TiO_2 emerged as a superior support compared to SiO_2. TiO_2's amphoteric nature facilitated better dispersion of H_3PMo, creating the potential possibility to synthesize a well-dispersed NH_4PMo catalyst (TN10, TN70) and enhancing catalytic activity and stability. By contrast, SiO_2-supported samples showed crystalline features of H_3PMo and NH_4PMo at higher loadings suggesting the presence of clusters.

Catalytic tests demonstrated that H_3PMo catalysts achieve high conversions and selectivity dependent on catalyst/reactant ratio, comparable to commercial NH_4PMo, but with no possibility of recyclability. When supported on TiO_2 and SiO_2, both catalysts exhibited significant conversion and recyclability. However, the cold filtration tests confirm the presence of leaching with an active

homogeneous phase for both bulk and SiO_2-supported samples. The TH70 and TN70 samples are the only ones that do not show leaching and provide relevant results. Uncertainties remain regarding the nature of this active phase and whether the solid phase contributes to the reaction. This homogeneous phase may eventually re-precipitate or not, potentially reforming a recyclable catalyst depending on its nature [56].

Despite the presence of leaching and the uncertainty surrounding this active phase, the tunability of Keggin structures highlight their promise for DODH applications. The ability to modify the composition and properties of Keggin-based catalysts provides a flexible platform for future optimization.

Finally, several new perspectives emerge from this work: (1) Demonstrate the synthesis of a well-dispersed NH_4PMo sample on a support. TiO_2 appearing to be the best candidate, though other supports such as MnO_2, which has an isoelectric point intermediate between TiO_2 and SiO_2, should also be tested. This can be achieved by using TPD-NH_3 to analyze a sample already neutralized with NH_3 via the optimal synthesis method to detect NH_3 desorption. And also, through XPS and ICP-AES analysis by calculating the N/P atomic ratio. (2) Investigate why the amount of catalyst affects the selectivity of the reaction in DODH by detecting and identifying the other products of the reaction. (3) Identify the nature of the active phase in DODH.

Bibliography

[1] Y. Nakagawa, M. Yabushita, et K. Tomishige, « A perspective on catalytic production of olefinic compounds from biomass », *RSC Sustain.*, vol. 1, n° 4, p. 814-837, 2023, doi: 10.1039/D3SU00033H.

[2] F. Salem, « Bioenergy Biomass to Biofuels and Waste to Energy-Academic Press (2020) », doi: https://www.academia.edu/76316521/Bioenergy_Biomass_to_Biofuels_and_Waste_to_Energy_Academic_Press_2020_

[3] B. E. Sharkey, « Development and Characterization of Robust and Cost-Effective Catalysts for Selective Biomass Upgrading to Fuels and Chemicals by Deoxydehydration », mai 2020, doi: https://hdl.handle.net/20.500.14394/18193

[4] K. Tomishige, G. W. Huber, T. Wang, et T. Mizugaki, « Preface to the special issue on "Catalytic conversion of biomass to fuels and chemicals" », *Fuel Processing Technology*, vol. 201, p. 106343, mai 2020, doi: 10.1016/j.fuproc.2020.106343.

[5] F. Jentoft, « Transition metal-catalyzed deoxydehydration: missing pieces of the puzzle », *Catalysis Science & Technology*, vol. 12, janv. 2022, doi: 10.1039/D1CY02083H.

[6] C. Muzyka et J.-C. M. Monbaliu, « Perspectives for the Upgrading of Bio-Based Vicinal Diols within the Developing European Bioeconomy », *ChemSusChem*, vol. 15, n° 5, p. e202102391, 2022, doi: 10.1002/cssc.202102391.

[7] C. P. Nicholas, « Applications of light olefin oligomerization to the production of fuels and chemicals », *Applied Catalysis A: General*, vol. 543, p. 82-97, août 2017, doi: 10.1016/j.apcata.2017.06.011.

[8] J. C. Mol, « Industrial applications of olefin metathesis », *Journal of Molecular Catalysis A: Chemical*, vol. 213, n° 1, p. 39-45, avr. 2004, doi: 10.1016/j.molcata.2003.10.049.

[9] D. Sathe, S. Yoon, Z. Wang, H. Chen, et J. Wang, « Deconstruction of Polymers through Olefin Metathesis », *Chemical Reviews*, vol. 124, n° 11, p. 7007-7044, 2024, doi: 10.1021/acs.chemrev.3c00748.

[10] X. Geng *et al.*, « Recent progress on non-noble metal catalysts for the deoxydehydration of biomass-derived oxygenates », *Green Processing and Synthesis*, vol. 12, n° 1, janv. 2023, doi: 10.1515/gps-2023-0129.

[11] E. Aksanoglu, Y. H. Lim, et R. A. Bryce, « Direct Deoxydehydration of Cyclic

trans-Diol Substrates: An Experimental and Computational Study of the Reaction Mechanism of Vanadium(V)-based Catalysis** », *ChemSusChem*, vol. 14, n° 6, p. 1545-1553, 2021, doi: 10.1002/cssc.202002594.
[12] K. DeNike, « Catalytic Activity of Tungsten-dioxo and Tungsten-diimido Complexes », *Graduate Theses and Dissertations*, august 2022, doi: https://scholarworks.uark.edu/etd/4584
[13] K. DeNike et S. Kilyanek, « Deoxydehydration of vicinal diols by homogeneous catalysts: a mechanistic overview », *Royal Society Open Science*, vol. 6, p. 191165, nov. 2019, doi: 10.1098/rsos.191165.
[14] S. Qu, Y. Dang, M. Wen, et Z.-X. Wang, « Mechanism of the methyltrioxorhenium-catalyzed deoxydehydration of polyols: a new pathway revealed », *Chemistry*, vol. 19, n° 12, p. 3827-3832, march 2013, doi: 10.1002/chem.201204001.
[15] Y.-Y. Jiang, J.-L. Jiang, et Y. Fu, « Mechanism of Vanadium-Catalyzed Deoxydehydration of Vicinal Diols: Spin-Crossover-Involved Processes », *Organometallics*, vol. 35, p. 3388-3396, oct. 2016, doi: 10.1021/acs.organomet.6b00602.
[16] C. Canote, « Proton-Coupled Electron Transfer to Drive Biomass Conversion », *Graduate Theses and Dissertations*, august 2024, [doi: https://scholarworks.uark.edu/etd/5403
[17] G. Chapman et K. M. Nicholas, « Vanadium-catalyzed deoxydehydration of glycols », *Chem. Commun.*, vol. 49, n° 74, p. 8199, 2013, doi: 10.1039/c3cc44656e.
[18] « New solid oxo-rhenium and oxo-molybdenum catalysts for the deoxydehydration of glycols to olefins | Request PDF », *ResearchGate*, oct. 2024, doi: 10.1016/j.cattod.2017.05.090.
[19] R. Tran et S. M. Kilyanek, « Deoxydehydration of polyols catalyzed by a molybdenum dioxo-complex supported by a dianionic ONO pincer ligand », *Dalton Trans.*, vol. 48, n° 43, p. 16304-16311, 2019, doi: 10.1039/C9DT03759D.
[20] J. Li, M. Lutz, M. Otte, et R. J. M. Klein Gebbink, « A Cptt-Based Trioxo-Rhenium Catalyst for the Deoxydehydration of Diols and Polyols », *ChemCatChem*, vol. 10, n° 20, p. 4755-4760, 2018, doi: 10.1002/cctc.201801151.
[21] S. Liu *et al.*, « Mechanism of MTO-Catalyzed Deoxydehydration of Diols to Alkenes Using Sacrificial Alcohols », *Organometallics*, vol. 32, n° 11, p. 3210-3219, juin 2013, doi: 10.1021/om400127z.
[22] J. R. Dethlefsen, D. Lupp, B.-C. Oh, et P. Fristrup, « Molybdenum-Catalyzed Deoxydehydration of Vicinal Diols », *ChemSusChem*, vol. 7, n° 2, p. 425-428, 2014, doi: 10.1002/cssc.201300945.
[23] B. E. Sharkey, A. L. Denning, F. C. Jentoft, R. Gangadhara, T. V. Gopaladasu, et K. M. Nicholas, « New solid oxo-rhenium and oxo-molybdenum catalysts for the deoxydehydration of glycols to olefins », *Catalysis Today*, vol. 310, p. 86-93,

juill. 2018, doi: 10.1016/j.cattod.2017.05.090.
[24] K. M. Nicholas, « Carbon Monoxide (CO)- and Hydrogen-Driven, Vanadium-Catalyzed Deoxydehydration of Glycols », févr. 2016, doi: 10.1021/acscatal.5b02667.
[25] R. T. Larson *et al.*, « Hydrogen Gas-Mediated Deoxydehydration/Hydrogenation of Sugar Acids: Catalytic Conversion of Glucarates to Adipates », *J. Am. Chem. Soc.*, vol. 139, nº 40, p. 14001-14004, oct. 2017, doi: 10.1021/jacs.7b07801.
[26] A. L. Denning, H. Dang, Z. Liu, K. M. Nicholas, et F. C. Jentoft, « Deoxydehydration of Glycols Catalyzed by Carbon-Supported Perrhenate », *ChemCatChem*, vol. 5, nº 12, p. 3567-3570, déc. 2013, doi: 10.1002/cctc.201300545.
[27] N. Ota, M. Tamura, Y. Nakagawa, K. Okumura, et K. Tomishige, « Performance, Structure, and Mechanism of ReO_x–Pd/CeO_2 Catalyst for Simultaneous Removal of Vicinal OH Groups with H_2 », *ACS Catal.*, vol. 6, nº 5, p. 3213-3226, mai 2016, doi: 10.1021/acscatal.6b00491.
[28] Y. Nakagawa *et al.*, « Mechanistic Study of Hydrogen-Driven Deoxydehydration over Ceria-Supported Rhenium Catalyst Promoted by Au Nanoparticles », *ACS Catal.*, vol. 8, nº 1, p. 584-595, janv. 2018, doi: 10.1021/acscatal.7b02879.
[29] J. I. Michael McClain et K. M. Nicholas, « Elemental Reductants for the Deoxydehydration of Glycols », *ACS Catal.*, vol. 4, nº 7, p. 2109-2112, juill. 2014, doi: 10.1021/cs500461v.
[30] S. Vkuturi, G. Chapman, I. Ahmad, et K. M. Nicholas, « Rhenium-catalyzed deoxydehydration of glycols by sulfite », *Inorg Chem*, vol. 49, nº 11, p. 4744-4746, juin 2010, doi: 10.1021/ic100467p.
[31] M. Kumar et K. Gayen, « Developments in biobutanol production: New insights », *Applied Energy*, vol. 88, nº 6, p. 1999-2012, juin 2011, doi: 10.1016/j.apenergy.2010.12.055.
[32] J. R. Dethlefsen, D. Lupp, A. T. Gorfo, L. B. Nielsen, et P. Fristrup, « Molybdenum-catalyzed conversion of diols and biomass-derived polyols to alkenes using isopropyl alcohol as reductant and solvent », *ACS Catalysis*, vol. 5, nº 6, p. 3638-3647, 2015, doi: 10.1021/acscatal.5b00427.
[33] J. Li, M. Lutz, et R. J. M. K. Gebbink, « N,N,O-Coordinated tricarbonylrhenium precatalysts for the aerobic deoxydehydration of diols and polyols », *Catalysis Science & Technology*, vol. 10, nº 11, p. 3782-3788, 2020, doi: 10.1039/D0CY00618A.
[34] J. S. Reinhold, J. Pang, B. Zhang, F. E. Kühn, et T. Zhang, « Rhenium-based catalysts for biomass conversion », *Green Chem.*, vol. 26, nº 21, p. 10661-10686, oct. 2024, doi: 10.1039/D4GC02925A.
[35] L. Sandbrink, E. Klindtworth, H.-U. Islam, A. M. Beale, et R. Palkovits, « ReO

$_x$ /TiO_2 : A Recyclable Solid Catalyst for Deoxydehydration », *ACS Catal.*, vol. 6, n° 2, p. 677-680, févr. 2016, doi: 10.1021/acscatal.5b01936.
[36] L. Sandbrink *et al.*, « Supported Molybdenum Catalysts for the Deoxydehydration of 1,4-Anhydroerythritol into 2,5-Dihydrofuran », *ChemSusChem*, vol. 10, n° 7, p. 1375-1379, 2017, doi: 10.1002/cssc.201700010.
[37] N. Ota, M. Tamura, Y. Nakagawa, K. Okumura, et K. Tomishige, « Hydrodeoxygenation of vicinal OH groups over heterogeneous rhenium catalyst promoted by palladium and ceria support », *Angew Chem (Int Ed Engl)*, vol. 54, n° 6, p. 1897-1900, févr. 2015, doi: 10.1002/anie.201410352.
[38] K. M. Kwok *et al.*, « Hydrogen-Free Gas-Phase Deoxydehydration of 2,3-Butanediol to Butene on Silica-Supported Vanadium Catalysts », *ChemCatChem*, vol. 9, n° 13, p. 2443-2447, 2017, doi: 10.1002/cctc.201700301.
[39] M. T. Pope, « Polyoxo Anions: Synthesis and Structure », in *Reference Module in Chemistry, Molecular Sciences and Chemical Engineering*, Elsevier, 2013, p. B978012409547201043X. doi: 10.1016/B978-0-12-409547-2.01043-X.
[40] J. J. Borrás-Almenar, E. Coronado, A. Müller, et M. Pope, Éd., *Polyoxometalate Molecular Science*. Dordrecht: Springer Netherlands, 2003. doi: 10.1007/978-94-010-0091-8.
[41] C. Lang, J. Schnee, B. J. T. Mba, F. Devred, et E. M. Gaigneaux, « Ammonium-substitution for successfully activating the bulk of Keggin acid salts in 1-butanol dehydration », *Catal. Sci. Technol.*, vol. 10, n° 18, p. 6244-6256, sept. 2020, doi: 10.1039/D0CY00820F.
[42] A. Magerat, S. Hermans, et E. Gaigneaux, « A novel versatile platform as efficient deoxydehydration (DODH) catalysts: Keggin polyoxometalates », 9 juillet 2024, *ChemRxiv*. doi: 10.26434/chemrxiv-2024-23d4q.
[43] I. V. Kozhevnikov, « Catalysis by Heteropoly Acids and Multicomponent Polyoxometalates in Liquid-Phase Reactions », *Chem. Rev.*, vol. 98, n° 1, p. 171-198, févr. 1998, doi: 10.1021/cr960400y.
[44] P. Cannon, « A critical study of the precipitation of ammonium phospho-12-molybdate », *Talanta*, vol. 3, n° 3, p. 219-231, janv. 1960, doi: 10.1016/0039-9140(60)80023-9.
[45] D. W. Archer et R. B. Helslop, « The solubility of ammonium 12-molybdophosphate in dilute acids », *Analytica Chimica Acta*, vol. 30, p. 582-589, janv. 1964, doi: 10.1016/S0003-2670(00)88770-X.
[46] J. Schnee, A. Eggermont, et E. M. Gaigneaux, « Boron Nitride: A Support for Highly Active Heteropolyacids in the Methanol-to-DME Reaction », *ACS Catal.*, vol. 7, n° 6, p. 4011-4017, juin 2017, doi: 10.1021/acscatal.7b00808.
[47] A. Alasmari, R. Al-Faze, E. F. Kozhevnikova, et I. V. Kozhevnikov, « Solid acid catalysts comprising heteropoly acids supported on SiO2, TiO2 and ZrO2: A microcalorimetric investigation of catalyst acidity and new insight into the mechanism of alcohol dehydration over HPA », *Catalysis Communications*, vol.

180, p. 106710, juill. 2023, doi: 10.1016/j.catcom.2023.106710.
[48] J. North *et al.*, « Efficient hydrodesulfurization catalysts based on Keggin polyoxometalates », *Applied Catalysis A: General*, vol. 508, p. 16-24, nov. 2015, doi: 10.1016/j.apcata.2015.10.001.
[49] E. I. García-López, G. Marcì, I. Krivtsov, J. Casado Espina, L. F. Liotta, et A. Serrano, « Local Structure of Supported Keggin and Wells–Dawson Heteropolyacids and Its Influence on the Catalytic Activity », *J. Phys. Chem. C*, vol. 123, n° 32, p. 19513-19527, août 2019, doi: 10.1021/acs.jpcc.9b03659.
[50] M. H. Alizadeh, M. Mirzaei, et H. Razavi, « 2D-network of inorganic–organic hybrid material built on Keggin type polyoxometallate and amino acid: $[L\text{-}C_2H_6NO_2]_3[(PO_4)Mo_{12}O_{36}]\cdot 5H_2O$ », *Materials Research Bulletin*, vol. 43, n° 3, p. 546-555, mars 2008, doi: 10.1016/j.materresbull.2007.04.018.
[51] S. K. Ghosh, V. K. Perla, K. Mallick, et T. Pal, « Ammonium phosphomolybdate: a material for dielectric crossover and resistive switching performance », *Nanoscale Adv.*, vol. 2, n° 11, p. 5343-5351, 2020, doi: 10.1039/D0NA00481B.
[52] K. Fukaya, A. Srifa, E. Isikawa, et H. Naruke, « Synthesis and structural characterization of polyoxometalates incorporating with anilinium cations and facile preparation of hybrid film », *Journal of Molecular Structure*, vol. 979, n° 1, p. 221-226, august 2010, doi: 10.1016/j.molstruc.2010.06.030.
[53] B. E. Givens, Z. Xu, J. Fiegel, et V. H. Grassian, « Bovine serum albumin adsorption on SiO2 and TiO2 nanoparticle surfaces at circumneutral and acidic pH: A tale of two nano-bio surface interactions », *Journal of Colloid and Interface Science*, vol. 493, p. 334-341, mai 2017, doi: 10.1016/j.jcis.2017.01.011.
[54] M. M. Schubert, S. Hackenberg, A. C. van Veen, M. Muhler, V. Plzak, et R. J. Behm, « CO Oxidation over Supported Gold Catalysts—“Inert” and “Active” Support Materials and Their Role for the Oxygen Supply during Reaction », *Journal of Catalysis*, vol. 197, n° 1, p. 113-122, jan. 2001, doi: 10.1006/jcat.2000.3069.
[55] G. Socrates, *Infrared and Raman Characteristic Group Frequencies: Tables and Charts*. John Wiley & Sons, 2004.
[56] B. E. Sharkey et F. C. Jentoft, « Fundamental Insights into Deactivation by Leaching during Rhenium-Catalyzed Deoxydehydration », *ACS Catal.*, vol. 9, n° 12, p. 11317-11328, dec. 2019, doi: 10.1021/acscatal.9b02806.
As a tool for translation and reformulation:
OpenAI. *ChatGPT (Jan Version)*. OpenAI, 2025, https://openai.com

Appendices

Mechanisms and Impact of Acetalization on DODH

Acetalization is a reaction in which an alcohol reacts with an aldehyde or ketone to form an acetal or ketal [12], respectively (Figure A (ii) (iii) (iv)). This reaction occurs in the presence of an acid catalyst and involves dehydration, releasing one molecule of water. Acetalization poses a significant challenge to the deoxydehydration (DODH) process by directly interfering with its efficiency and selectivity. DODH relies on vicinal diols as substrates to produce alkenes through the elimination of water and an oxygen atom, facilitated by a metal-oxo catalyst. However, when acetalization occurs, the diols are consumed to form acetals (in cases where the substrate acts as a reductant, the carbonyl groups can react with the alcohols present in the solution) which are thermodynamically stable and do not participate further in the catalytic cycle. This diversion reduces the availability of diol substrates required for the DODH reaction.

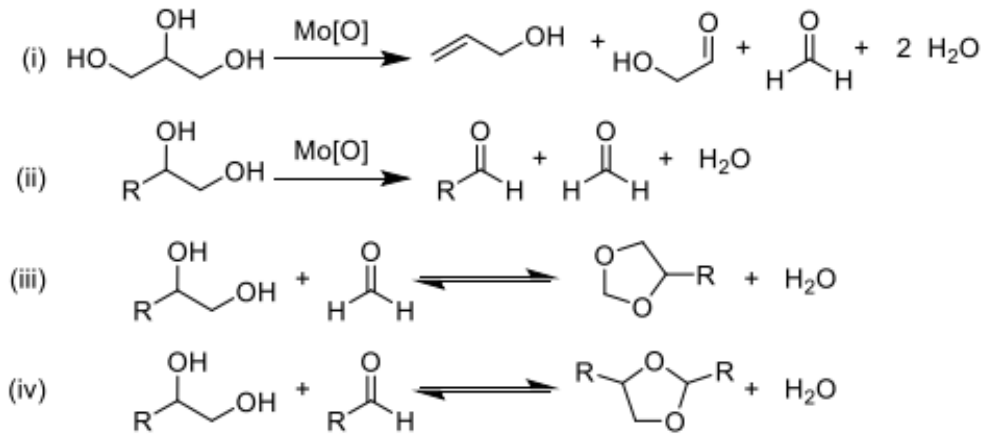

Figure A: Oxidative deformylation of glycerol and acetal formation of diols [12].

The presence of acetals also introduces unwanted complexity, as they create additional byproducts that complicate the isolation and purification of the

desired alkene products. Additionally, acetalization can interfere with the metal-oxo catalyst by potentially binding to the active sites, further diminishing the catalytic efficiency.

Infrared spectroscopy

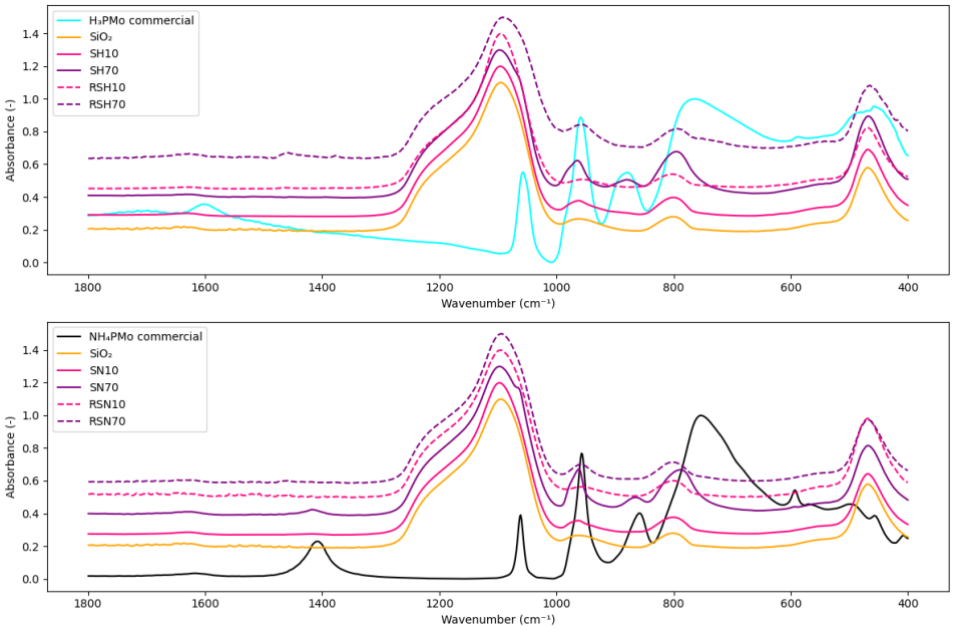

Figure B: Infrared spectra of samples supported on SiO_2 compared to H_3PMo and NH_4PMo.

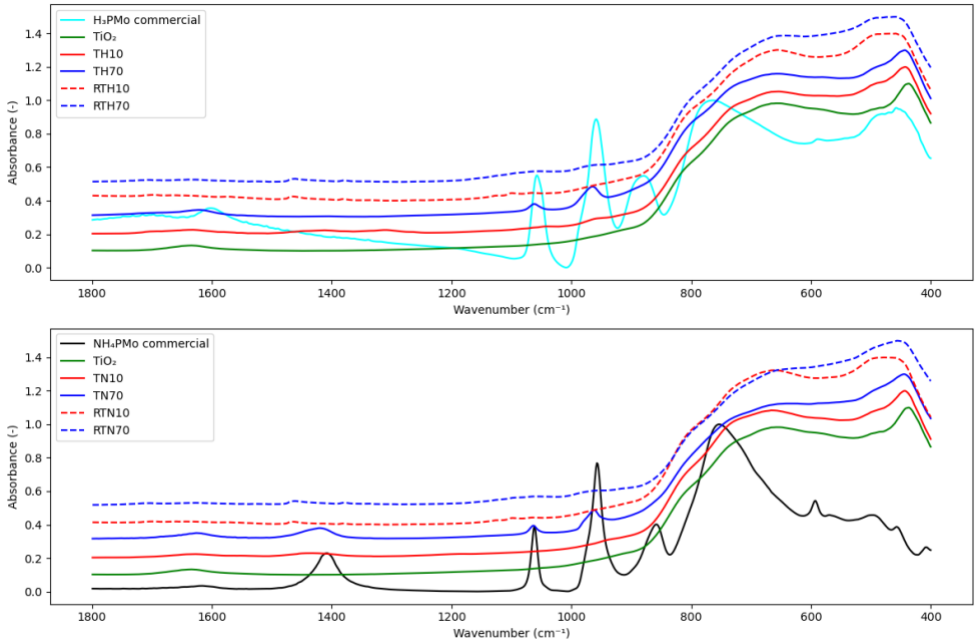

Figure C: Infrared spectra of samples supported on TiO_2 compared to H_3PMo and NH_4PMo.

Highly dispersed Keggin phosphomolybdates as deoxydehydration catalysts

Presented by Sébastien BAFFREY

The realization that fossil fuel sources are finite have sparked a major research effort into the use of renewable biomass as a feedstock for chemicals and fuels. Deoxydehydration (DODH) appears to be an interesting reaction as it enables the conversion of biomass depolymerization products into highly functionalizable olefins.

This work investigated the development of ammonium phosphomolybdate ($(NH_4)_3PMo_{12}O_{40}$ = NH_4PMo) catalysts for the DODH of vicinal diols, exploring their potential as cost-effective and recyclable alternatives to rhenium-based catalysts. Through a systematic approach, the synthesis of both bulk and supported NH_4PMo catalysts was optimized using a strategy involving the neutralization of phosphomolybdic acid ($H_3PMo_{12}O_{40}$ = H_3PMo) with NH_3 and a subsequent posttreatment consisting of heating the sample at different temperatures after this neutralization. Posttreatment at 300°C was identified as critical for achieving the targeted product. PXRD, UV-Vis and IR spectroscopy, confirmed the structural integrity and chemical features of the synthesized catalysts. Bulk NH_4PMo demonstrated recyclability, unlike H_3PMo. However, the study also highlighted that the active phase primarily operates in a homogeneous manner, irrespective of the catalyst form. This behavior underscores a key limitation in realizing a fully heterogeneous system. TiO_2 and SiO_2 were evaluated as supports. TiO_2 facilitated better dispersion of H_3PMo and exhibited higher catalytic performance compared to SiO_2, likely due to its amphoteric nature. Samples supported on SiO_2 displayed evidence of leaching, with catalytic activity observed during cold filtration tests, further supporting the predominance of a homogeneous mechanism.

Finally, further research is needed to detect the nature of the active catalyst phase and determine whether it can be reused and optimized to enhance its activity, minimize its leaching, and explore alternative support materials to maximize their industrial applicability.

UNIVERSITÉ CATHOLIQUE DE LOUVAIN
Faculté des bioingénieurs
Croix du Sud, 2 bte L7.05.01, 1348 Louvain-la-Neuve, Belgique | **www.uclouvain.be/agro**